Title: Somatic Activating Mutations in *Pik3ca* Cause Sporadic Venous Malformations in Mice and Humans

Authors: Sandra D. Castillo[1,*], Elena Tzouanacou[2,3], May Zaw-Thin[4], Inma M. Berenjeno[1], Victoria E.R. Parker[5], Iñigo Chivite[6], Maria Milà-Guasch[1], Wayne Pearce[1], Isabelle Solomon[1], Ana Angulo-Urarte[6], Ana M. Figueiredo[6], Robert E. Dewhurst[2], Rachel G. Knox[5], Graeme R. Clark[7], Cheryl L. Scudamore[8], Adam Badar[4], Tammy L. Kalber[4], Julie Foster[9], Daniel J. Stuckey[4], Anna L. David[10], Wayne A. Phillips[11], Mark F. Lythgoe[4], Valerie Wilson[2], Robert K. Semple[5], Neil J. Sebire[12], Veronica A. Kinsler[12], Mariona Graupera[6],† & Bart Vanhaesebroeck[1,*,†]

Affiliations:
[1]UCL Cancer Institute, University College London, London WC1E 6BT, UK
[2]MRC Centre for Regenerative Medicine, School of Biological Sciences, The University of Edinburgh, Edinburgh EH16 4UU, UK
[3]Institut Pasteur, Département de Biologie du Developpement, CNRS URA 2578, 75724 Paris, France
[4]Centre for Advanced Biomedical Imaging, University College London, London WC1E 6BT, UK
[5]Institute of Metabolic Science, University of Cambridge, Addenbrooke's Hospital, Cambridge CB2 0QQ, UK
[6]Vascular Signaling Laboratory, Institut d´Investigació Biomèdica de Bellvitge (IDIBELL), 08908 L´Hospitalet de Llobregat, Barcelona, Spain
[7]Department of Medical Genetics, School of Clinical Medicine, University of Cambridge, Cambridge CB2 0SP, UK
[8]Mary Lyon Centre, MRC Harwell, Harwell OX11 0RD, UK.
[9]Barts Cancer Institute, Queen Mary University of London, London EC1M 6BQ, UK
[10]UCL Institute for Women's Health, London WC1E 6BT, UK
[11]Surgical Oncology Research Laboratory, Peter MacCallum Cancer Centre, Melbourne VIC 3002, Australia
[12]Great Ormond Street Hospital for Children, NHS Foundation Trust, London WC1N 3JH, UK

* To whom correspondence should be addressed: S.D.C. (sandra.castillo@ucl.ac.uk) or B.V. (bart.vanh@ucl.ac.uk)

†Joint Last Authors

One Sentence Summary: Mutant *Pik3ca* gives rise to venous malformations

Abstract

Venous malformations (VMs) are painful and deforming vascular lesions composed of dilated vascular channels, present from birth. Mutations in the *TEK* gene, encoding the tyrosine kinase

receptor TIE2, are found in approximately half of sporadic (non-familial) VMs, and the causes of the remaining cases are unknown. Sclerotherapy, widely accepted as first-line treatment, is not fully efficient, and targeted therapy for this disease remains underexplored. In this study, we have generated a mouse model that faithfully mirrors human VM through mosaic expression of *Pik3ca*^{H1047R}, a constitutively active mutant of the p110α isoform of PI 3-kinase (PI3K), in the embryonic mesoderm. Endothelial expression of *Pik3ca*^{H1047R} resulted in endothelial cell (EC) hyperproliferation, reduction in pericyte coverage of blood vessels, and decreased expression of arteriovenous specification markers. PI3K pathway inhibition with rapamycin normalized endothelial cell hyperproliferation and pericyte coverage in postnatal retinas and stimulated VM regression *in vivo*. In line with the mouse data, we also report the presence of activating *PIK3CA* mutations in human VMs, mutually exclusive with *TEK* mutations. Our data demonstrate a causal relationship between activating *Pik3ca* mutations and the genesis of VMs, provide a genetic model that faithfully mirrors the normal etiology and development of this human disease, and establish the basis for the use of PI3K-targeted therapies in VMs.

Introduction

Enzymes in the PI3K family signal downstream of a variety of cell surface receptors to regulate multiple cellular functions, including growth and proliferation *(1)*. The p110α isoform of phosphoinositide 3-kinase (PI3K), encoded by the *PIK3CA* (OMIM 171834) gene, is frequently activated through mutation in cancer *(2)*. Similar activating mutations in *PIK3CA* have recently been linked to non-cancerous disease conditions, such as a spectrum of regional overgrowth disorders *(3-6)* [which have now been designated under the umbrella term *PIK3CA*-Related Overgrowth Spectrum (PROS) disease *(7)*] and isolated (not associated with overgrowth) lymphatic malformations (LMs) *(8)*. In these conditions, the *PIK3CA* mutations are present from birth and occur in a mosaic pattern, mainly in tissues of mesodermal origin. This contrasts with somatic

PIK3CA mutations in cancer, which are almost exclusively present in epithelial tissues. The *PIK3CA* mutations present in PROS and LMs are similar to those found in solid tumors, with the H1047R mutation in the catalytic domain being the most prevalent *(8,9*). In this study, we report the presence of somatic activating *PIK3CA* mutations in another human disease condition of mesodermal origin, namely isolated VMs. In addition, we created a genetically-modified mouse model that displays mutant *Pik3ca*-driven congenital vascular malformations with features pathognomonic for human VMs.

VMs are the most common vascular malformations, with an overall incidence of 1/5000 *(10*). VMs are usually congenital lesions that consist of dilated venous channels with scarce mural cell coverage. These VMs can be of different sizes and be present in any tissue, such as subcutaneous tissue or internal organs. VMs are painful and disfiguring, with many causing bleeding and obstruction of organs, and in some cases localized intravascular coagulopathy and pulmonary embolism *(11,12*). Treatment of VMs mainly consists of alleviation of symptoms with compression garments when possible, and curative treatment is seldom achievable. At present, sclerotherapy is the mainstay therapy to diminish the volume of VMs, but it causes a variety of side effects and is not fully effective *(12*).

Mutations in the *TEK* gene, which codes for the endothelial tyrosine kinase receptor TIE2, are known to cause about half of sporadic VMs *(13*); the cause of the other half remains unknown. Here, in a cohort of patients diagnosed with sporadic VMs, without any associated overgrowth, we found *PIK3CA*-activating mutations in a mutually exclusive manner to previously identified mutations in *TEK (14)*. This was corroborated by a study in the accompanying paper by Castel *et al*. *(15*), in which *PIK3CA* mutations were found in 25% of the VMs analysed, again in a mutually exclusive manner to *TEK* mutations. The finding that activating mutations in *PIK3CA* play a key role in the pathogenesis of VMs provides guidance for refined diagnosis for this disease and a possible targeted therapeutic intervention with PI3K pathway inhibitors.

Results

Mosaic *Pik3ca*^{H1047R} expression in embryonic mesoderm causes VMs in mice

In this study, we set out to investigate the effects of *Pik3ca* mutation in mesodermal tissue in mice. Given that all known disease conditions of mesodermal origin currently associated with *PIK3CA* mutations are congenital or early childhood onset, we induced expression of mutant *Pik3ca* in the embryonic mesoderm. To more precisely model the human disease context, mutant *Pik3ca* expression was induced in a mosaic fashion, in the heterozygous state and from its endogenous promoter *(16*). We reasoned that such tissue-restricted mosaic induction could also avoid the detrimental effects of ubiquitous expression of mutant *Pik3ca* during embryonic mouse development *(17*). The mutant used for these experiments was *Pik3ca*^{H1047R}, which encodes the H1047R hot-spot mutation found in cancer *(2*), LMs *(8*) and PROS *(9*).

For these studies, we generated a mouse line (referred to as *T-CreER*^{T2}) by introducing a transgene (Fig. S1A) that drives the expression of a 4-hydroxytamoxifen (4-OHT)-inducible Cre recombinase under the control of the previously characterized promoter of the *T* gene *(18*). The *T* gene encodes the Brachyury transcription factor that is transiently expressed in the nascent embryonic mesoderm *(19*). To evaluate Cre activity, we crossed *T-CreER*^{T2} mice with *Rosa26-lacZ* reporter mice *(20*) that ubiquitously express the floxed *lacZ* gene expression cassette from the *Rosa26* locus (Fig. S1B), and stained for lacZ expression after treatment of mice with 4-OHT. We administered 4-OHT to pregnant females between embryonic day (E) 7.5 and 10.5. In line with the known temporal expression of the *T* gene *(19*), induction of Cre produced a widespread lacZ expression in the mesoderm, which was highest at E7.5 (Fig. S1C). Cre activity at E7.5 was dependent on the 4-OHT dose and was present in a mosaic pattern, except at the higher doses tested (Fig. S1D).

We next crossed *T-CreER^{T2}* mice to mice that are heterozygous for a Cre-inducible knock-in allele of *Pik3ca^{H1047R} (16*), followed by mosaic *Pik3ca^{H1047R}* induction at E7.5 with different doses of 4-OHT (Fig. 1A). Several of these mice [hereafter referred to as MosMes-*Pik3ca^{H1047R}* (Mosaic Mesodermal-*Pik3ca^{H1047R}*) mice] but not *T-CreER^{T2};Pik3ca^{WT}* (hereafter referred to as WT) littermate mice, were born with subcutaneous vascular malformations in different body sites (Fig. 1B). No apparent overgrowth was observed in other tissues, nor alterations in body weight, organ size or tissue histology (tested up to 6 months of age), compared to WT littermate mice that had also been treated with 4-OHT (Fig. S2; Table S1). This phenotype was not fully penetrant at lower 4-OHT doses, but increased in a dose-dependent manner (Table S2). The lower doses of 4-OHT tested gave rise to localized vascular lesions, whereas the higher doses, possibly because of the higher probability of targeting multiple EC progenitors, induced multifocal, diffuse, and more severe malformations (Fig. 1B). High 4-OHT doses also resulted in a lower than expected Mendelian distribution of mutant mice (Table S3), with some of the mutant embryos displaying vascular developmental defects (Fig. S3). Our observations on the lethality and vascular defects in MosMes-*Pik3ca^{H1047R}* embryos are similar to the previously reported phenotypes of ubiquitous or EC-specific expression of *Pik3ca^{H1047R}* in the developing embryo *(17*).

Computed Tomography Angiography (CT-A) analysis of adult MosMes-*Pik3ca^{H1047R}* mice confirmed the presence of subcutaneous vascular malformations and revealed additional internal vascular malformations in the mesentery and urogenital area (Fig. 1C,D). Some of these mice displayed rectal bleeding and phlebectasias of the portal vein and inferior *vena cava* (Fig. 1C), similar to those observed in patients with venous vascular malformations (reviewed in *(21*)).

Additional scanning of blood flow in the vascular malformation by power Doppler ultrasound indicated that the contribution of flow was primarily venous in origin (slow flow) (Fig. S4). This was corroborated by histological analysis which showed that the vascular lesions in MosMes-*Pik3ca^{H1047R}* mice were poorly circumscribed, non-encapsulated lesions composed of blood-filled,

predominantly thin-walled, irregular and variably sized blood vessels interposed between normal tissues (Fig. 1D). Some blood vessels contained organising fibrin thrombi, with focal interstitial hemorrhage present. Immunostaining of these vascular lesions for lymphatic markers (LYVE-1, PROX-1) revealed the presence of malformed lymphatic vessels (Fig. S5), however, the lymphatic component was much less prominent than the aberrant blood vessels. This is similar with what is seen in humans, where purely vascular malformations are rare and usually contain a mixture of vessel types, with some types being pathologically prominent such as the blood vessels in the case of VMs *(22*).

Altogether, these observations point to a diagnosis of VMs in MosMes-*Pik3ca*^{H1047R} mice, with a pathology and disease burden remarkably similar to those observed in humans with VMs.

PIK3CA **is mutated in human VMs**

Having identified the causative role of activating *Pik3ca* mutation in VMs in mice, we explored the presence of *PIK3CA* mutations in human VMs. We analysed *PIK3CA* and *TEK* genes by deep sequencing (mean coverage of 2000x) in human sporadic VMs that had no associated overgrowth or other predominant vascular malformation component. Among the VMs sequenced, 3/13 (23%) were mutant for *PIK3CA* (Fig. 2) and 6/13 (46%) for *TEK*, with an allelic frequency of 4-13% (Table 1). Interestingly, mutations in *PIK3CA* and *TEK* were mutually exclusive. The observed *PIK3CA* mutations are hot-spot mutations in cancer *(2*), PROS *(9*) and LMs *(8*), with the observed *TEK* mutations having previously been described for VMs *(23*). In line with our observations, Castel *et al*. in the accompanying manuscript *(15*) found that *PIK3CA* was mutated in 25% of VM cases. Taken together, these findings indicate that *PIK3CA* mutation status could be a relevant diagnostic marker for human VMs and corroborate a causal role of *PIK3CA* mutation in VM generation.

Endothelial activation of *Pik3ca* promotes hyperproliferation in ECs and impairs pericyte coverage

ECs, being the main cell type in the microvasculature, are thought to be important in VM development. Given the key role for *Pik3ca* in EC biology *(24-28*), we decided to selectively test the impact of *Pik3ca*^{H1047R} expression in ECs using postnatal retina as a model of angiogenesis. To this end, we generated EC-*Pik3ca*^{H1047R} mice by crossing conditional heterozygous *Pik3ca*$^{WT/H1047R}$ mice onto *Pdgfb-iCreER* mice that express 4-OHT-inducible Cre specifically in ECs *(29*) (Fig. S6). 4-OHT was administered to EC-*Pik3ca*^{H1047R} pups on postnatal day 1 (P1), and retinal angiogenesis was analyzed five days later (Fig. 3A). Staining of P6 retinas with isolectin-B_4 (IB4, which binds specifically to the EC plasma membrane) revealed that endothelial expression of *Pik3ca*^{H1047R} resulted in dramatic hyperplasia, with individual vessels no longer being discernible, correlating with increased proliferation and numbers of ECs (Fig. 3B, C). This increase in EC number was confirmed by the higher levels *VE-Cadherin* in EC-*Pik3ca*^{H1047R} retinas Fig. S7). Radial expansion of the vascular bed was also decreased upon endothelial expression of *Pik3ca*^{H1047R}, possibly due to EC hyperplasia (Fig. 3D, E), whereas sprouting angiogenesis, as measured by number and length of sprouts, was not affected (Fig. 3D, F). In addition, at P9, when mouse retinas have started vascular remodeling, EC-*Pik3ca*^{H1047R}-driven hyperplasia persisted, and there was no difference in apoptosis (as assessed by expression of cleaved caspase-3) between EC-*Pik3ca*^{H1047R} and *Pik3ca*^{WT} retinas (**Fig. S8**), indicating that there was no compensation of *Pik3ca*^{H1047R}-driven hyperplasia by enhanced apoptosis during the remodeling process.

A distinctive feature of human VMs is the low number, or even absence, of mural cells *(30*). Proper homeostasis of vessels requires a tight interplay between ECs and their supporting mural cells, which are perivascular cells of two types, vascular smooth muscle cells (vSMCs) and pericytes. Both cell types are differently distributed over the vasculature, with vSMCs typically present in large vessels and pericytes mainly localized in the microvasculature *(31*). In EC-

Pik3ca^{H1047R} retinas at P6, pericytes (NG2-positive cells) were conspicuously absent from the vascular front and very sparse in the plexus, where they were poorly associated with the vessels, in contrast with *Pik3ca*^{WT} retinas that showed a typical attachment of pericytes to the EC surface with multiple extensions (Fig. 3G, H). Defective mural cell coverage was also observed in the VMs from MosMes-*Pik3ca*^{H1047R} mice (Fig. 1D).

PDGF-B, which is produced by ECs, is the major attractant for pericytes *(32*) and is present in lower amounts in human *TEK*-mutant VMs *(33*). The FOXO1 transcription factor, which is negatively regulated by PI3K activity, stimulates PDGF-B expression. In line with this, analysis of total mRNA isolated from retinas and lungs (a tissue highly enriched in ECs) from postnatal P6 mice showed a decrease in *Pdgfb* expression in EC-*Pik3ca*^{H1047R} mice compared to *Pik3ca*^{WT} mice (**Fig. 3I, S9A**). The pericyte phenotype observed in EC-*Pik3ca*^{H1047R} retinas is reminiscent of that observed in the so-called *Pdgfb*-retention motif knock-out mice, in which PDGF-B produced by the ECs is not retained at the cell surface *(34*).

Throughout development and in adult life, arteriovenous specification in ECs is associated with selective expression of specific genes *(35*). The mRNA expression of three proteins known to be key in this process, namely COUP-TFII (encoded by the *Nr2f2* gene) and Eph-B4 (encoded by the *Ephb4* gene), which are expressed in venous ECs, and Ephrin-B2 (encoded by the *Efnb2* gene), which is selectively expressed in arterial ECs, was reduced in EC-*Pik3ca*^{H1047R} postnatal retinas and lungs compared to those in *Pik3ca*^{WT} mice (Fig. 3J, S9B). This finding indicates that endothelial expression of *Pik3ca*^{H1047R} compromises arteriovenous identity of ECs.

Taken together, our findings show that *Pik3ca*^{H1047R} expression in ECs results in EC hyperproliferation, defective pericyte coverage, and loss of arteriovenous identity.

Rapamycin reduces *Pik3ca*^{H1047R} EC hyperproliferation and prevents loss of pericyte coverage

At the moment, there are no targeted therapies for VMs. Rapamycin and its analogs interfere with signaling downstream of PI3K by inhibition of mTOR *(36*) and are approved for compassionate use in human therapy of vascular anomalies *(37-43*). To test the effect of rapamycin on *Pik3ca*^{H1047R} ECs *in vivo*, we treated EC-*Pik3ca*^{H1047R} pups with rapamycin first at P1 (administered together with 4-OHT) followed by a second injection at P5 (8 h before analysis of retinal angiogenesis; Fig. 4A). Drug treatment prevented retinal vascular hyperplasia, reduced the number of ECs and proliferation (Fig. 4B, C), and normalized pericyte coverage in both the vascular front and plexus of EC-*Pik3ca*^{H1047R} retinas (Fig. 4D). Rapamycin also decreased vessel area and number of ECs in *Pik3ca*^{WT} retinas, with a borderline reduction in EC proliferation (Fig. 4B, C), in line with its previously documented anti-angiogenic effects *(44*).

Rapamycin induces regression of *Pik3ca*^{H1047R}-driven VMs *in vivo*

To take these observations closer to the disease context, adult MosMes-*Pik3ca*^{H1047R} mice with VMs were treated with rapamycin (Table 2). The rapamycin dose chosen for this study (4 mg/kg every other day) was based on previous studies using long-term rapamycin treatment *(45,46*). In WT mice, this dose was found to have no detectable impact on overall health, weight, or behavior (Table 2). Due to different degrees of severity of the VMs, only mice that were deemed to be sufficiently fit to tolerate the treatment were included. The mice recruited to this therapeutic experiment had subcutaneous VMs that were heterogeneous in size and location, in some cases accompanied with phlebectasias of main internal veins (inferior *vena cava*, portal vein). Two weeks of rapamycin treatment resulted in a ~25% reduction in the volume of the VMs, as assessed by CT-A (Fig. 5, S10), with a cessation of bleeding from the VM or anus shortly after the start of the treatment with rapamycin. Continued treatment showed progressive regression of the VMs (Fig. 5, Fig. S10). Overall, these observations are in line with data from a study on VM patients with a wide range of lesions, in which a heterogeneous response to rapamycin treatment was observed, with

reduction in VM volume between 10-20%, resulting in symptom improvement and clinical benefit *(43*).

Overall, our data suggest that PI3K pathway intervention might be an effective therapeutic option for human *PIK3CA*-driven VMs.

Discussion

Here we identify the presence of activating *PIK3CA* mutations in human VMs and report a genetic mouse model for this disease. We demonstrate that somatic, mosaic expression of an activating mutation (H1047R) in *Pik3ca* in the embryonic mesoderm of mice can induce and maintain VMs. Previous mouse models of VM have used transgenic expression of a murine viral oncogene *(47*) or xenotransplantation into nude mice of either human vascular endothelial cells (HUVECs) transduced with mutant *TEK (43*) or the MS1 immortalized endothelial cell line expressing mutant AKT1 *(48*). Xenograft models do not take into account the developmental origin and natural progression of the human disease nor the complex admixture of vessel and stromal cells in human VM lesions. They also show full regression upon rapamycin treatment, which was not observed in our mouse models, in which regression was very variable after long-term treatment, in line with observations in human VM patients *(43*). The xenograft models may therefore be a less predictive model for the human disease. Yet, our mosaic mesodermal VM mouse model shows some limitations for use in standardized uniform cohort therapeutic experiments, namely some degree of embryo lethality, a variable penetrance of the VM phenotype, and a large heterogeneity of VMs in terms of size, localization, and expansion. However, these limitations of our mouse model adequately reflect the characteristics of this human disease, with every patient showing a distinct disease pattern, progression, and response to therapy, most likely resulting from the spatially and temporally distinct and mosaic acquisition of the mutation causing the disease. Of note, activation of PI3K signaling in adult mice, either by ubiquitous expression of mutant *Pik3ca* from its

endogenous promoter *(49*) or EC-specific expression of transgenic activated *Akt1 (50*) increases blood vessel size without inducing VMs. This underscores the concept that VMs arise as a result of genetic errors during embryonic development.

Mechanistically, our data suggest that VMs are likely to develop as a result of *Pik3ca*^{H1047R}-induced enhancement of EC proliferation during embryonic vasculogenesis. Indeed, EC hyperproliferation during vasculogenesis has previously been shown to give rise to vessel hyperfusion, and to result in dilated, dysfunctional vessels, similar to those found in VMs *(51,52*). Another typical feature of VMs is poor mural cell coverage *(30*). We also show that *Pik3ca*^{H1047R} expression in ECs inhibits pericyte attachment, likely because of the decreased expression of PDGF-B, which is necessary for pericyte coverage *(53*). This might therefore also contribute to the genesis of VMs upon *Pik3ca* mutation. Lastly, *Pik3ca*^{H1047R} might also contribute to the formation of VMs by preventing arteriovenous differentiation, as seen by decreased expression of arteriovenous differentiation markers *(54*). It is therefore tempting to speculate that VMs could be the result of hyperproliferation of ECs and lack of maturation of primitive capillary beds as a consequence of PI3K pathway overactivation.

At present, it is not clear why widespread mosaic induction of *Pik3ca*^{H1047R} in the mouse mesoderm gives rise to malformations solely in the vasculature and does not induce obvious overgrowth or malformation in other tissue compartments. This might be due to the chosen strategy (timing and tissue location) of *Pik3ca*^{H1047R} gene induction. However, Castel *et al*. in the accompanying manuscript *(15*) have made similar observations in their models. One explanation could be the previously reported exceptional sensitivity of ECs to PI3K pathway deregulation *(24-28*).

Human genetic data presented here and in the accompanying manuscript *(15*) reveal the presence of *PIK3CA* mutations in VMs, mutually exclusive with mutations in the *TEK* gene that were discovered over 20 years ago *(30*). Our studies thus uncover and document the potential for a

new targeted therapy in human VMs, and the potential for repurposing of p110α inhibitors currently being developed for cancer treatment. An important consideration is how diagnosis of *TEK* and *PIK3CA* mutations in VMs can influence the treatment of this disease using targeted agents. The wild-type TIE2 receptor tyrosine kinase is known to signal through both the PI3K and MAPK signaling pathways in ECs *(55,56*). Both pathways have been implicated in signaling downstream of mutant TIE2 in ECs, with their relative contribution to biological outputs not being clear at present *(14,33,43*). *TEK*-mutant cells surprisingly do not respond to TIE2 kinase inhibitors *(43*), possibly because mutant TIE2 kinase is not very responsive to drugs that were developed against the wild-type TIE2. *TEK*-mutant cells show chronic activation of the PI3K and MAPK pathways and respond very well to inhibition of each of these pathways *(14*). Our studies identify a subpopulation of patients with *PIK3CA*-mutant VMs, which will most likely be non-responsive to TIE2 or MAPK inhibitors. However, like the *TEK*-mutant VMs *(43*), *PIK3CA*-mutant VMs are expected to respond to PI3K inhibitors or rapamycin. It is also likely that *TEK*-mutant VMs will benefit from treatment with PI3K inhibitors in combination with MAPK inhibitors.

In conclusion, our findings in mice allowed us to discover the presence of *PIK3CA* mutations in a human disease. VMs join the growing list of diseases where the presence of activating *PIK3CA* mutations, commonly associated with cancer, results in tissue malformation without causing malignancy *(8,9*). Our finding that mutation in *PIK3CA* plays a key role in the pathogenesis and maintenance of VMs provides guidance for improved diagnosis for this disease and a possible targeted therapeutic avenue using PI3K pathway inhibitors.

Materials and Methods

Study design

This study was designed to test the effect of *Pik3ca*^{H1047R} expression in the embryonic mesoderm of mice. We obtained sufficient data on mice to determine that this results in VMs. To translate these findings to the human context, we tested for *PIK3CA* mutation in human VMs and found that this gene is mutated in this disease. For this, well-characterized patients with confirmed VMs and without any associated overgrowth or malformation were recruited at Great Ormond Street Hospital, London, UK. All patients provided informed consent. In addition, to better understand the mechanisms underlying the role of *Pik3ca*^{H1047R} in ECs, we performed mouse retinal angiogenesis studies as a vascular biology read-out. For these experiments, we performed a power analysis on preliminary data, suggesting that a minimal cohort size of n=4-6 is necessary to observe a significant difference with 80% power, depending on the type of experiment. The sample size for each experiment is indicated in the corresponding figure legend. Given that n was <10, non-parametric tests were applied. All mechanistic studies were performed without randomization or blinding. Exclusion criteria were only applied to data shown in Fig. 4 (rapamycin treatment of mouse harboring VMs): only mice that were deemed to be sufficiently fit to tolerate the treatment were included in the experiment. This is in line with UK Home Office regulations.

Subjects

This study was approved by the UK National Research Ethics Committee. Written informed consent was obtained from all participants or their parents. Tissues from individuals diagnosed as having sporadic VMs, not associated with other syndromes, were investigated. Genomic DNA was extracted from lesions using standard procedures.

Next generation sequencing with preceding target enrichment

Sequencing of *TEK* and *PIK3CA* was performed using Next Generation Sequencing with preceding target enrichment. All equipment and materials were purchased from Life Technologies, Thermo-Fisher Scientific. In brief, DNA was quantified using Qubit, and libraries were prepared using the Ion AmpliSeq Library 96 Kit 2.0 with 10 ng of genomic DNA in each reaction. This involved an initial PCR reaction to amplify genomic targets using a custom-designed primer pool which provides coverage of all coding regions of *PIK3CA* and *TEK* (primer sequences available upon request). Samples were then partially digested before ligation of barcode adaptors and emulsion PCR. Enrichment steps were carried out using the Ion OneTouch 200 Template Kit v2, the amplicon libraries were sequenced on an Ion Torrent Personal Genome Machine system using 318 chips, and bar-coding was applied with an Ion Xpress Barcode Adapters 1–16 Kit. Ion Reporter software was used to analyze data, or alternatively Bam files were uploaded and viewed in the Integrative Genomics Viewer, Broad Institute (http://www.broadinstitute.org/igv/). The mean depth of coverage for sequencing was 2000X.

Reagents

Primary antibodies to the following proteins were used: Erg (ab92513; Abcam), NG2 (AB5320; Merck Millipore), endomucin (sc-65495; Santa Cruz Biotechnology), LYVE-1 (AF2125; R&D Systems), PROX-1 (PRB-238C; Covance), and Cleaved caspase-3 (9664S; Cell Signalling Technology). Secondary antibodies conjugated to Cy3, Cy5, or AlexaFluor 647 were from Jackson ImmunoResearch Laboratories. For immunohistochemistry (IHC), biotinylated antibodies were from Vector Laboratories. Isolectin GS-IB_4 conjugated to AlexaFluor 488 (I21411) or AlexaFluor 568 (I21412) (further referred to as IB4) was from Life Technologies. Immu-Mount mounting medium was from Thermo Scientific. AuroVist 15 nm gold nanoparticles were from Nanoprobes

Inc. Rapamycin used for therapeutic studies was obtained from Merck Millipore. All chemicals, unless otherwise stated, were from Sigma-Aldrich.

Mice

Mice were housed in individually-ventilated cages and cared for according to UK Home Office guidelines and legislation, with procedures accepted by the Ethics Committees of University College London and Queen Mary University of London. All mice used were backcrossed on a C57BL/6 background for more than 12 generations. *Pik3ca*$^{WT/H1047R}$ mice harbor a germline *Pik3ca* allele with a conditional H1047R mutation *(16)*. In these mice, Lox*P* sites flank exon 20 of *Pik3ca*, which, upon Cre recombination, is replaced by a downstream copy of exon 20 containing a CAT to AGG change in codon 1047. *Pdgfb-iCreER* mice *(29)* express an inducible iCreER recombinase from the endogenous *Pdgfb* locus.

Generation of the *T-CreER*^{T2} mouse line

The pTcreER^{T2} vector (Fig. S1), comprising the *T* regulatory sequence from -1050 bp to +140 bp *(18)* was inserted upstream of a *CreER*^{T2} sequence. To eliminate uninduced background activity of Cre in the absence of 4-OHT, the *nls* sequence at the 5' of *CreER*^{T2} was removed. This plasmid was *FspI*-linearized and electroporated into E14TG2a ES cells as described previously *(57)*. After 10 days of selection with hygromycin (140 μg/ml), resistant clones were isolated, expanded, and screened by Southern blot to verify integration of the transgene and to identify ES clones with single and multiple insertions of the transgene. Clones were tested in parallel by *in situ* hybridisation for Cre expression in differentiating ES cells. Four clones (three with a single integration and one with two integrations) that showed the characteristic spatial pattern of *T* expression in differentiating ES cell monolayers *(58)* were selected for further analysis. Absence of uninduced background recombination and 4-OHT-induced Cre recombination in these four clones

were tested *in vitro* by transient transfection of a Cre-conditional Egfp transgene (pPHCAG-C2-egfp, a gift from Austin G. Smith, Wellcome Trust, Medical Research Council Cambridge Stem Cell Institute, UK). Clones with single *T-CreER^{T2}* integration showed efficient recombination upon treatment with 0.2 μM or 1 μM of 4-OHT, with virtually no background of uninduced recombination. These clones were injected into C57BL/6 host blastocysts and chimeric male offspring mated to C57BL/6 females. F1 heterozygotes were identified by coat color and PCR amplification of the Cre sequence. Offspring were backcrossed for >5 generations to C57BL/6 mice before generating a homozygote *T-CreER^{T2}* line by intercrossing. After further characterization by crosses with *Rosa26-lacZ* reporter mice *(20)*, one *T-CreER^{T2}* mouse line (number 53) was maintained and established in the homozygote state.

Mesoderm- and EC-specific *Pik3ca^{H1047R}* expression in mice

Mesoderm-specific mosaic expression of *Pik3ca^{H1047R}* (MosMes-*Pik3ca^{H1047R}* mice) was achieved by crossing *Pik3ca$^{WT/H1047R}$* mice with *T-CreER^{T2}* mice. To induce mosaic Cre activation, pregnant females were given varying doses of 4-OHT (12.5 to 250 μg, from a stock solution of 10 mg/ml, diluted in 1:1 absolute ethanol-Kolliphor EL), with 200 μl of PBS added for intraperitoneal injection at E7.5 (E0.5 relates to the presence of a vaginal plug indicating that the mating occurred the night before). Progesterone (dissolved in Kolliphor EL) was co-administered at half the total dose of 4-OHT, to avoid undesirable estrogen agonist effects of 4-OHT, which can result in late fetal abortions in pregnant mice. Postnatal EC-specific expression of *Pik3ca^{H1047R}* was achieved by crossing *Pik3ca$^{WT/H1047R}$* with *Pdgfb-iCreER* mice. To induce Cre activation, newborn pups (P1) were injected intragastrically with 5 μg 4-OHT (dissolved in absolute ethanol).

Histology and IHC

Mouse tissues and VMs were fixed in 4% PFA and embedded in paraffin. 5 μm sections were stained with hematoxylin-eosin using standard histology procedures. Immunostaining was performed using the automated Discovery XT slide staining system (Ventana Medical Systems) at the Molecular Cytology Core in Memorial Sloan Kettering Cancer Center (New York, USA). Briefly, tissue sections were deparaffinised with EZPrep buffer, and antigen retrieval was performed with CC1 buffer (Ventana Medical Systems). Sections were blocked for 30 min. with Background Buster solution (Innovex) (for PROX-1 antibody) or 10% rabbit serum (for LYVE-1 antibody) followed by endogenous avidin/biotin blocking for 8 min. Then, sections were incubated with specific antibodies for 3 h, followed by incubation with biotinylated secondary antibodies. All slides were scanned using Zeiss Mirax Midi digital slide scanner.

Whole-mount embryo X-gal staining

Freshly isolated E12.5 embryos were fixed in 4% paraformaldehyde on ice for 30 min, washed (3 x 10 min) in PBT (PBS with 0.1% Tween), and stained for 48 h at 30ºC in X-gal staining solution (4 mM potassium ferricyanide, 4 mM potassium ferrocyanide, 2 mM $MgCl_2$, and 1 mg/ml X-gal in PBT). After staining, embryos were washed (3 x 10 min) in PBS, post-fixed in 4% paraformaldehyde for ≥ 1 h and mounted.

Whole-mount embryo immunofluorescence

Freshly isolated E9.5 embryos were fixed in 4% paraformaldehyde overnight at 4°C. After washing in PBT, embryos were dehydrated in increasing concentrations of methanol (50%, 80% methanol/PBT, 100% methanol), rehydrated in decreasing concentrations of methanol, then washed for 30 min in Pblec buffer (0.2 mM $CaCl_2$, 0.2 mM $MgCl_2$, 0.2 mM $MnCl_2$, and 2% Triton X-100 in PBS) and incubated overnight at 4°C with antibody to endomucin, diluted 1:20 in Pblec. After five washes in PBT, embryos were incubated with Cy5-labeled secondary antibody diluted 1:100 in

PBS, 0.5% BSA, 0.25% Tween-20. Finally, embryos were washed three times in PBS, post-fixed for 1 min in 4% paraformaldehyde, and mounted.

Mouse imaging by CT-A

Mice were anesthetized with an isoflurane/O_2 mix and tail vein cannulated for the delivery of approximately 0.1 ml of gold nanoparticles per 25 g of mouse weight. Animal temperature was maintained at 37°C, with monitoring and maintenance of respiration at 60 breaths/min. Mice were placed in the supine position 4 h after injection of gold nanoparticles and whole body CT scans were acquired using a nanoScanPET/CT scanner (Mediso) with a 50 kVP X-ray source and 300 ms exposure time in 720 projections with an acquisition time of 15 min. CT images were reconstructed in voxel size 68 x 68 x 68 μm using Nucline (Mediso) software. Image analysis and 3D visualization was performed using VivoQuant (inviCRO version 1.23patch3) software.

Mouse imaging by Doppler ultrasound

A Vevo 2100 imaging station (VisualSonics Inc.) was used for ultrasound imaging. A VisualSonics MS-550D (central frequency 40 MHz, axial resolution 40 μm, lateral resolution 90 μm, image depth 15 mm, image width 14 mm) was used for data acquisition. Mice were anesthetized with an isoflurane/O_2 mix and placed on a heated imaging stage maintained at 37°C. The body temperature, heart rate, and respiratory rate were closely monitored throughout each imaging session. Abdominal hair was removed using a depilatory cream (Veet, Reckitt Benckiser) and rinsed with warm water. Pre-warmed ultrasound gel (UltrasoundGel.co.uk) was then placed on the abdomen. Flow velocity waveforms of vascular lesions were obtained by locating with color Doppler, power Doppler, and then placing the pulsed wave Doppler sample gate within the vessels and at the appropriate angle relative to flow direction. 2D-guided M-mode images were obtained to measure maximum vessel diameter. Images were analyzed with the VisualSonics Vevo 2100 software package.

Retinal angiogenesis

Newborn pups (P1) were injected intragastrically with 5 µg 4-OHT dissolved in absolute ethanol at 5 mg/ml. P6 eyes were harvested and fixed for 1 h in 4% PFA at 4°C and washed in PBS. Retinas were dissected, stained with IB4 and flat-mounted, or processed for immunostaining *(59)*. For immunostaining, fixed retinas were blocked and permeabilized with blocking buffer (1% BSA, 0.3% Triton X-100 in PBS) for 4 h at 4°C, then incubated overnight at 4°C with the corresponding primary antibodies [anti-Erg (1/300), anti-NG2 (1/200), anti-Cleaved-caspase 3 (1/50)] in blocking buffer and washed in PBT (3 x 10 min). After 30 min incubation in Pblec, retinas were incubated for 2 h with the corresponding labelled secondary antibody and IB4 in Pblec, washed with PBT (3 x 10 min), post-fixed with 4% paraformaldehyde for 1 min, and flat-mounted.

***In vivo* EC proliferation**

Pups were injected intraperitoneally with 50 µl of EdU (diluted to 2 mM in 1:1 DMSO-PBS) 2 h before harvesting of the eyes. EdU was detected with Click IT EdU Alexa Fluor-647 (Life Technologies) according to the manufacturer's instructions. Retinas were then labelled with the corresponding antibodies and IB4 as described above. Retinas were imaged with a Zeiss LSM 700 confocal microscope. EdU-positive nuclei were counted as proliferating ECs in a 100 μm^2 region at the angiogenic front or plexus using the ImageJ software.

RNA extraction and quantitative PCR

Total RNA was extracted from P6 mouse retinas and lungs using the RNeasy Plus MiniKit (#74134, QIAGEN) according to the manufacturer's protocol. Samples were quality-controlled and quantified using a Nanodrop ND-100 spectrophotometer. Reverse transcription of total RNA was performed using a High-Capacity cDNA Reserve Transcription Kit (#4368814, Applied

BiosystemsTM). Real-time quantitative PCR was performed using TaqMan Gene Expression Assays (Applied Biosystems) and the proprietary TaqMan Gene Expression assay FAM/TAMRA primers (Applied Biosystems) for *Pdgfb* (Mm00440678_m1), *Ephb4* (Mm00438750_m1), *Efnb2* (Mm01215897_m1), *Nr2f2* (Mm00772789_m1), *Cadh5* (Mm00486938_m1), and *Hprt* (Mm00446968_m1). *Pdgfb*, *Ephb4*, *Efnb2*, and *Nr2f2* mRNA expression in retinas was normalized to the mRNA of the EC-specific *Cdh5* (VE-Cadherin) housekeeping gene.

In vivo rapamycin treatment

Rapamycin was dissolved at 10 mg/ml in absolute ethanol and used for intraperitoneal injection in pups at P1 and P6 at 4 mg/kg. For adult mice, the 10 mg/ml stock of rapamycin in absolute ethanol was dissolved further in 5% polyethylene glycol (PEG-400) and 5% Tween-80 in PBS to 0.5 mg/ml. Mice were dosed with 4 mg rapamycin per kg by intraperitoneal injection every other day for a total of 28 days. This dose was based on previous studies using long-term rapamycin treatment *(45,46)*.

Statistics

GraphPad Prism 6 was used for all statistical analysis. Means were compared between two groups using the nonparametric Mann–Whitney U test. All statistical tests and sample size have been indicated in the figure legends.

List of Supplemental Materials

References and Notes:

1. B. Vanhaesebroeck, L. Stephens, P. Hawkins, PI3K signalling: the path to discovery and understanding. *Nature reviews. Molecular cell biology* **13**, 195-203 (2012).
2. Y. Samuels *et al.*, High frequency of mutations of the PIK3CA gene in human cancers. *Science* **304**, 554 (2004).
3. K. C. Kurek *et al.*, Somatic mosaic activating mutations in PIK3CA cause CLOVES syndrome. *American journal of human genetics* **90**, 1108-1115 (2012).
4. M. J. Lindhurst *et al.*, Mosaic overgrowth with fibroadipose hyperplasia is caused by somatic activating mutations in PIK3CA. *Nature genetics* **44**, 928-933 (2012).
5. J. B. Riviere *et al.*, De novo germline and postzygotic mutations in AKT3, PIK3R2 and PIK3CA cause a spectrum of related megalencephaly syndromes. *Nature genetics* **44**, 934-940 (2012).
6. J. H. Lee *et al.*, De novo somatic mutations in components of the PI3K-AKT3-mTOR pathway cause hemimegalencephaly. *Nature genetics* **44**, 941-945 (2012).
7. K. M. Keppler-Noreuil *et al.*, PIK3CA-related overgrowth spectrum (PROS): Diagnostic and testing eligibility criteria, differential diagnosis, and evaluation. *American journal of medical genetics. Part A* **167**, 287-295 (2015).
8. V. L. Luks *et al.*, Lymphatic and other vascular malformative/overgrowth disorders are caused by somatic mutations in PIK3CA. *The Journal of pediatrics* **166**, 1048-1054 e1041-1045 (2015).
9. K. M. Keppler-Noreuil *et al.*, Clinical delineation and natural history of the PIK3CA-related overgrowth spectrum. *American journal of medical genetics. Part A* **164A**, 1713-1733 (2014).
10. M. Uebelhoer, L. M. Boon, M. Vikkula, Vascular anomalies: from genetics toward models for therapeutic trials. *Cold Spring Harbor perspectives in medicine* **2** (2012).
11. C. E. Oduber, V. E. Gerdes, C. M. van der Horst, P. Bresser, Vascular malformations as underlying cause of chronic thromboembolism and pulmonary hypertension. *Journal of plastic, reconstructive & aesthetic surgery : JPRAS* **62**, 684-689; discussion 689 (2009).
12. A. Dompmartin, M. Vikkula, L. M. Boon, Venous malformation: update on aetiopathogenesis, diagnosis and management. *Phlebology / Venous Forum of the Royal Society of Medicine* **25**, 224-235 (2010).
13. N. Limaye *et al.*, Somatic mutations in angiopoietin receptor gene TEK cause solitary and multiple sporadic venous malformations. *Nature genetics* **41**, 118-124 (2009).
14. M. Natynki *et al.*, Common and specific effects of TIE2 mutations causing venous malformations. *Human molecular genetics* **24**, 6374-6389 (2015).
15. P. Castel *et al.*, Somatic PIK3CA mutations as a driver of sporadic venous malformations.
16. K. M. Kinross *et al.*, An activating Pik3ca mutation coupled with Pten loss is sufficient to initiate ovarian tumorigenesis in mice. *The Journal of clinical investigation* **122**, 553-557 (2012).
17. L. M. Hare *et al.*, Heterozygous expression of the oncogenic Pik3ca(H1047R) mutation during murine development results in fatal embryonic and extraembryonic defects. *Developmental biology* **404**, 14-26 (2015).
18. H. Yamaguchi, T. Niimi, Y. Kitagawa, K. Miki, Brachyury (T) expression in embryonal carcinoma P19 cells resembles its expression in primitive streak and tail-bud but not that in notochord. *Development, growth & differentiation* **41**, 253-264 (1999).
19. A. Kispert, B. G. Herrmann, Immunohistochemical analysis of the Brachyury protein in wild-type and mutant mouse embryos. *Developmental biology* **161**, 179-193 (1994).
20. P. Soriano, Generalized lacZ expression with the ROSA26 Cre reporter strain. *Nature genetics* **21**, 70-71 (1999).

21. S. Eifert, J. L. Villavicencio, T. C. Kao, B. M. Taute, N. M. Rich, Prevalence of deep venous anomalies in congenital vascular malformations of venous predominance. *Journal of vascular surgery* **31**, 462-471 (2000).
22. L. H. Lowe, T. C. Marchant, D. C. Rivard, A. J. Scherbel, Vascular malformations: classification and terminology the radiologist needs to know. *Seminars in roentgenology* **47**, 106-117 (2012).
23. J. Soblet, N. Limaye, M. Uebelhoer, L. M. Boon, M. Vikkula, Variable Somatic TIE2 Mutations in Half of Sporadic Venous Malformations. *Molecular syndromology* **4**, 179-183 (2013).
24. M. Graupera *et al.*, Angiogenesis selectively requires the p110alpha isoform of PI3K to control endothelial cell migration. *Nature* **453**, 662-666 (2008).
25. M. Graupera, M. Potente, Regulation of angiogenesis by PI3K signaling networks. *Experimental cell research* **319**, 1348-1355 (2013).
26. A. Soler *et al.*, Inhibition of the p110alpha isoform of PI 3-kinase stimulates nonfunctional tumor angiogenesis. *J Exp Med* **210**, 1937-1945 (2013).
27. L. M. Hare *et al.*, Heterozygous expression of the oncogenic Pik3caH1047R mutation during murine development results in fatal embryonic and extraembryonic defects. *Developmental biology* **404**, 14-26 (2015).
28. B. H. Jiang, J. Z. Zheng, M. Aoki, P. K. Vogt, Phosphatidylinositol 3-kinase signaling mediates angiogenesis and expression of vascular endothelial growth factor in endothelial cells. *Proceedings of the National Academy of Sciences of the United States of America* **97**, 1749-1753 (2000).
29. S. Claxton *et al.*, Efficient, inducible Cre-recombinase activation in vascular endothelium. *Genesis* **46**, 74-80 (2008).
30. M. Vikkula *et al.*, Vascular dysmorphogenesis caused by an activating mutation in the receptor tyrosine kinase TIE2. *Cell* **87**, 1181-1190 (1996).
31. E. R. Andreeva, I. M. Pugach, D. Gordon, A. N. Orekhov, Continuous subendothelial network formed by pericyte-like cells in human vascular bed. *Tissue & cell* **30**, 127-135 (1998).
32. P. Lindahl, B. R. Johansson, P. Leveen, C. Betsholtz, Pericyte loss and microaneurysm formation in PDGF-B-deficient mice. *Science* **277**, 242-245 (1997).
33. M. Uebelhoer *et al.*, Venous malformation-causative TIE2 mutations mediate an AKT-dependent decrease in PDGFB. *Human molecular genetics* **22**, 3438-3448 (2013).
34. P. Lindblom *et al.*, Endothelial PDGF-B retention is required for proper investment of pericytes in the microvessel wall. *Genes & development* **17**, 1835-1840 (2003).
35. S. F. Rocha, R. H. Adams, Molecular differentiation and specialization of vascular beds. *Angiogenesis* **12**, 139-147 (2009).
36. D. M. Sabatini, H. Erdjument-Bromage, M. Lui, P. Tempst, S. H. Snyder, RAFT1: a mammalian protein that binds to FKBP12 in a rapamycin-dependent fashion and is homologous to yeast TORs. *Cell* **78**, 35-43 (1994).
37. R. Loewe *et al.*, Stem cell marker upregulation in normal cutaneous vessels following pulsed-dye laser exposure and its abrogation by concurrent rapamycin administration: implications for treatment of port-wine stain birthmarks. *Journal of cutaneous pathology* **37 Suppl 1**, 76-82 (2010).
38. S. Kaylani, A. J. Theos, J. G. Pressey, Treatment of infantile hemangiomas with sirolimus in a patient with PHACE syndrome. *Pediatric dermatology* **30**, e194-197 (2013).
39. H. Yuksekkaya, O. Ozbek, M. Keser, H. Toy, Blue rubber bleb nevus syndrome: successful treatment with sirolimus. *Pediatrics* **129**, e1080-1084 (2012).
40. A. M. Hammill *et al.*, Sirolimus for the treatment of complicated vascular anomalies in children. *Pediatric blood & cancer* **57**, 1018-1024 (2011).

41. S. Riou *et al.*, Efficacy of rapamycin for refractory hemangioendotheliomas in Maffucci's syndrome. *Journal of clinical oncology : official journal of the American Society of Clinical Oncology* **30**, e213-215 (2012).
42. L. Marques *et al.*, Topical rapamycin combined with pulsed dye laser in the treatment of capillary vascular malformations in Sturge-Weber syndrome: phase II, randomized, double-blind, intraindividual placebo-controlled clinical trial. *Journal of the American Academy of Dermatology* **72**, 151-158 e151 (2015).
43. E. Boscolo *et al.*, Rapamycin improves TIE2-mutated venous malformation in murine model and human subjects. *The Journal of clinical investigation* **125**, 3491-3504 (2015).
44. M. Guba *et al.*, Rapamycin inhibits primary and metastatic tumor growth by antiangiogenesis: involvement of vascular endothelial growth factor. *Nature medicine* **8**, 128-135 (2002).
45. C. Chen, Y. Liu, P. Zheng, mTOR regulation and therapeutic rejuvenation of aging hematopoietic stem cells. *Science signaling* **2**, ra75 (2009).
46. Y. Fang *et al.*, Duration of rapamycin treatment has differential effects on metabolism in mice. *Cell metabolism* **17**, 456-462 (2013).
47. Y. A. Wang *et al.*, A novel transgenic mice model for venous malformation. *Transgenic research* **18**, 193-201 (2009).
48. B. Perry *et al.*, AKT1 overexpression in endothelial cells leads to the development of cutaneous vascular malformations in vivo. *Archives of dermatology* **143**, 504-506 (2007).
49. K. M. Kinross *et al.*, Ubiquitous expression of the Pik3caH1047R mutation promotes hypoglycemia, hypoinsulinemia, and organomegaly. *FASEB journal : official publication of the Federation of American Societies for Experimental Biology* **29**, 1426-1434 (2015).
50. T. L. Phung *et al.*, Pathological angiogenesis is induced by sustained Akt signaling and inhibited by rapamycin. *Cancer cell* **10**, 159-170 (2006).
51. C. J. Drake, C. D. Little, Exogenous vascular endothelial growth factor induces malformed and hyperfused vessels during embryonic neovascularization. *Proceedings of the National Academy of Sciences of the United States of America* **92**, 7657-7661 (1995).
52. C. J. Drake, C. D. Little, VEGF and vascular fusion: implications for normal and pathological vessels. *The journal of histochemistry and cytochemistry : official journal of the Histochemistry Society* **47**, 1351-1356 (1999).
53. M. Enge *et al.*, Endothelium-specific platelet-derived growth factor-B ablation mimics diabetic retinopathy. *The EMBO journal* **21**, 4307-4316 (2002).
54. H. U. Wang, Z. F. Chen, D. J. Anderson, Molecular distinction and angiogenic interaction between embryonic arteries and veins revealed by ephrin-B2 and its receptor Eph-B4. *Cell* **93**, 741-753 (1998).
55. M. J. Yoon *et al.*, Localization of Tie2 and phospholipase D in endothelial caveolae is involved in angiopoietin-1-induced MEK/ERK phosphorylation and migration in endothelial cells. *Biochemical and biophysical research communications* **308**, 101-105 (2003).
56. I. Kim *et al.*, Angiopoietin-1 regulates endothelial cell survival through the phosphatidylinositol 3'-Kinase/Akt signal transduction pathway. *Circulation research* **86**, 24-29 (2000).
57. E. Tzouanacou, S. Tweedie, V. Wilson, Identification of Jade1, a gene encoding a PHD zinc finger protein, in a gene trap mutagenesis screen for genes involved in anteroposterior axis development. *Molecular and cellular biology* **23**, 8553-8552 (2003).
58. C. Schmidt, V. Wilson, D. Stott, R. S. Beddington, T promoter activity in the absence of functional T protein during axis formation and elongation in the mouse. *Developmental biology* **189**, 161-173 (1997).

59. M. E. Pitulescu, I. Schmidt, R. Benedito, R. H. Adams, Inducible gene targeting in the neonatal vasculature and analysis of retinal angiogenesis in mice. *Nature protocols* **5**, 1518-1534 (2010).

Acknowledgements

The authors are especially grateful to the subjects who participated in this study, Maria Whitehead for expert assistance in the writing of the manuscript, Daniele Morelli for help with mouse experiments, Alex Virasami and Pau Castel for help with histopathology. Markus Fruttiger for *Pdgfb-iCreER* mice and Austin G. Smith for the pPHCAG-C2-egfp transgene.

Funding

Postdoctoral fellowships were from EMBO (ALTF 165-2013) to S.D.C, EU Marie Curie (MEIF-CT-2005-010264) to E.T. and EU Marie Curie (PIIF-GA-2009-252846) to I.M.B. M.Z.-T. is supported by the EPSRC Early Career Fellowship of T.L.K. (EP/L006472/1). D.J.S. is a BHF Intermediate Basic Science Research Fellow (FS/15/33/31608). A.L.D is supported by the UK NIHR Joint UCL/University College London Hospitals Biomedical Research Centre. V.E.R.P. was supported by the Wellcome Trust (097721/Z/11/Z). R.K.S. is supported by the Wellcome Trust (WT098498), the Medical Research Council (MRC_MC_UU_12012/5). R.G.K. is supported by the NIHR Rare Diseases Translational Research Collaboration. V.W. is supported by the European FPVI Integrated Project 'Eurostemcell'. M.F.L. and A.B. are supported by the King's College London and UCL Comprehensive Cancer Imaging Centre CR-UK and EPSRC, in association with the MRC and DoH (England). W.A.P. is supported by funding from the National Health and Medical Research Council (NHMRC) of Australia. Work in the laboratory of M.G. is supported by research grants SAF2013-46542-P and SAF2014-59950-P from MICINN (Spain), 2014-SGR-725 from the Catalan Government, the People Programme (Marie Curie Actions) from the European Union's Seventh Framework Programme FP7/2007-2013/ (REA grant agreement 317250), the Institute of Health Carlos III (ISC III) and the European Regional Development Fund (ERDF) under the integrated Project of Excellence no. PIE13/00022 (ONCOPROFILE). Work in the

laboratory of B.V. is supported by Cancer Research UK (C23338/A15965) and the UK NIHR University College London Hospitals Biomedical Research Centre.

Author contributions

S.D.C., M.G., and B.V. were the main contributors in the conception, design, acquisition and interpretation of the data and in writing the article. S.D.C., E.T., M.Z-T, I.M.B., V.E.R.P., I.C., M.M-G., W.P., I.S., A.A-U., A.M.F., R.E.D., R.G.K., and G.R.C. performed experiments and data analysis with input from V.W., R.K.S., M.G. and B.V. C.L.S. and N.J.S. interpreted histopathology. M.Z-T., A.B., T.L.K., J.F., D.J.S., A.L.D. and M.F.L were responsible for image analysis. W.A.P. provided a mouse reagent. V.A.K. liaised with human subjects, provided access to human tissue samples and conceptual input in the study.. S.D.C, M.G. and B.V. wrote the paper.

Competing financial interests

B.V. is consultant to Karus Therapeutics (Oxford, UK).

Figures

Figure 1. Mosaic expression of *Pik3ca^{H1047R}* in embryonic mouse mesoderm induces vascular malformations. (**A**) Genetic strategy for mosaic *Pik3ca^{H1047R}* induction in the embryonic mesoderm. *T-CreER^{T2}* mice were crossed with *Pik3ca$^{WT/H1047R}$* mice that have a germline *Pik3ca* allele with a conditional H1047R mutation in exon 20. Mosaic recombination in the mesoderm was induced by a single intra-peritoneal injection of a low dose of 4-OHT to pregnant mice at E7.5. (**B**) Left, E12.5 *T-CreER^{T2};R26-lacZ* mouse embryos from pregnant mice injected with the indicated dose of 4-OHT at E7.5 and stained for β-galactosidase (β-gal) activity. Right, Representative photographs of P1-P5 MosMes-*Pik3ca^{H1047R}* pups with congenital vascular malformations (indicated by arrows in the top panel), born to pregnant mice injected with the indicated 4-OHT dose at E7.5. (**C**) CT-A scans of adult mice four hours after intravenous injection of gold nanoparticles. The WT mouse (left) shows normal vascular anatomy, whereas MosMes-*Pik3ca^{H1047R}* mice display dilatation of the left common iliac vein (arrow) and VM in the urogenital area (asterisk) (mouse #1); subcutaneous VM (asterisk) and dilatation of the inferior *vena cava* (arrow) (mouse #2); subcutaneous and urogenital VMs (asterisks) and dilatation of the inferior *vena cava* and portal vein (arrows) (mouse #3). (**D**) Representative hematoxylin and eosin (H&E)-stained sections of subcutaneous (left) and deep mesenteric (right) VMs in MosMes-*Pik3ca^{H1047R}* mice, showing abnormal, enlarged, and irregular vascular channels, most containing blood and organising fibrin thrombi (T), some interposing between skeletal muscle (SM) and other tissue structures. No cytological atypia was observed. (P, pancreas).

Figure 2. *PIK3CA* is mutated in human VMs. (A) Patient 9 showing VMs (*PIK3CA^{H1047L}*) in the lower lip and tongue. (B) Patient 13 with VM (*PIK3CA^{E545K}*) in the left hand.

Figure 3. Endothelial activation of *Pik3ca* promotes hyperproliferation in ECs and impairs pericyte coverage. (**A**) Schematic of the 4-OHT and EdU administration regime used. (**B**) Representative flat-mounted *Pik3ca*^{WT} and EC-*Pik3ca*^{H1047R} P6 retinas stained with IB4 (red, revealing ECs) and antibody to the Erg transcription factor (nuclear marker of ECs; green) and labelled with EdU (blue). (**C**) Quantitative analysis of the retina vessel area (assessed by IB4 staining), EC numbers (assessed by staining for Erg), and number of proliferating ECs (cells positive for both EdU and Erg). Data represent mean ± SEM. **p ≤ 0.01 (Mann-Whitney U test). n=6/genotype. (**D**) Representative flat-mounted control and EC-*Pik3ca*^{H1047R} P6 retinas stained with IB4 and antibody to the Erg transcription factor. (**E**) Quantification of the radial expansion of vasculature in retinas. Data represent mean ± SEM. *p < 0.05 (Mann-Whitney U test). n=6/genotype. (**F**) Quantification of the number of sprouts at the vascular front per unit length, and the length of sprouts. Data represent mean ± SEM. n.s., not significant, p > 0.05 (Mann-Whitney U test). n=6/genotype. (**G**) Flat-mounted *Pik3ca*^{WT} and EC-*Pik3ca*^{H1047R} retinas showing vasculature (IB4; red) and pericytes (stained for NG2, a membrane proteoglycan found in pericytes; green). **Right**, higher magnification of highlighted sections. (**H**) Quantification of pericyte coverage in the vasculature of retinas (assessed by % of NG2 staining relative to IB4 staining). Data represent mean ± SEM. *p < 0.05 (Mann-Whitney U test). n=6/genotype. (**I**) *Pdgfb* mRNA expression in EC-*Pik3ca*^{H1047R} P6 retinas. Data represent mean ± SEM. **p < 0.01 (Mann-Whitney U test). n=5/genotype. (**J**) *Ephb4*, *Nr2f2*, and *Efnb2* mRNA expression in EC-*Pik3ca*^{H1047R} P6 retinas. Data represent mean ± SEM. n.s., not significant, p > 0.05, *p < 0.05, **p < 0.01 (Mann-Whitney U test). n=5/genotype.

Figure 4. Rapamycin reduces *Pik3ca*^{H1047R} EC hyperproliferation and prevents loss of pericyte coverage in postnatal retinas. (**A**) Schematic of the 4-OHT and rapamycin administration regime used for analysis of retinal angiogenesis. (**B**) Representative flat-mounted P6

retinas from vehicle and rapamycin-treated *Pik3ca*^{WT} and EC-*Pik3ca*^{H1047R} pups. Retinas are stained with IB4 (red) and antibody to the Erg transcription factor (green) and labeled with EdU (blue). (**C**) Quantitative analysis of the retinal vessel area (assessed by IB4 staining), EC numbers (assessed by staining for Erg), and number of proliferating ECs (cells positive for both EdU and Erg). Data represent mean ± SEM. n.s., not significant, $p>0.05$, *$p < 0.05$, **$p < 0.01$ (Mann-Whitney U test). n=6/genotype. (**D**) Representative flat-mounted P6 retinas from untreated *Pik3ca*^{WT} and EC-*Pik3ca*^{H1047R} pups and rapamycin-treated EC-*Pik3ca*^{H1047R} pups showing vasculature (IB4; red) and pericytes (stained for NG2; green). (**E**) Quantitative analysis of pericyte coverage in the vascular front and plexus of retinas (assessed by % of NG2 staining relative to IB4 staining). Data represent mean ± SEM. n.s., not significant, $p > 0.05$, *$p < 0.05$, **$p < 0.01$ (Mann-Whitney U test). n=6/genotype.

Figure 5. Rapamycin induces regression of *Pik3ca*^{H1047R}-driven VMs *in vivo.* (**A**) Measurement of the volume of the subcutaneous VM (circled in blue) from CT-A images of mouse #1 (Table 2), showing the volume of the VM. H, heart; L, liver; S, spleen. (**B**) Measurement of the average diameter of the inferior vena cava and portal vein from CT-A images of an untreated WT mouse and a MosMes-*Pik3ca*^{H1047R} littermate mouse, before and after 2 and 4 weeks of rapamycin treatment. IVC, inferior vena cava; PV, portal vein.

Table 1. *PIK3CA* and *TEK* mutations in human sporadic VMs

Patient	1	2	3	4	5	6	7	8	9	10	11	12	13
Age	4 years	20 years	3 years	15 years	3 years	10 years	9 years	15 years	14 years	10 years	20 years	3 years	6 years
Sex	M	M	M	M	F	F	F	F	F	F	F	M	M
Location of VM	Upper lip	Sole of foot	Scapular area	Arm, chest, extensive	Face	Cheek	Face	Arm	Tongue, lower lip, neck	Tongue, lower lip	Hand	Foot	Hand
PIK3CA	WT	E545K	WT	WT	WT	WT	WT	WT	H1047L	WT	WT	WT	E545K
Percent *PIK3CA* mutant allele	*NA*	6%	*NA*	*NA*	*NA*	*NA*	*NA*	*NA*	4%	*NA*	*NA*	*NA*	4%
TEK	G1115X	WT	Y897C, R918H	WT	WT	WT	L914F	L914F	WT	L914F	WT	Y897C, R918S	WT
Percent *TEK* mutant allele	9%	*NA*	5%	*NA*	*NA*	*NA*	4%	13%	*NA*	5%	*NA*	11%	*NA*

NA: not applicable

Table 2. Treatment of MosMes-*Pik3ca*^{H1047R} mice with rapamycin

Mouse #	**1**	**2**	**3**	**4**	**5**	**6**
Sex	m	m	m	f	m	f
Phenotype	Subcutaneous VM at right flank, phlebectasia of portal vein and inferior vena cava	Subcutaneous VM at left flank, phlebectasia of portal vein and inferior vena cava	Subcutaneous VM at the base of the tail, below left hind limb	Phlebectasia of portal vein and inferior vena cava. No VM detected by CT-A.	WT control	WT control
Age at starting treatment*	8-week-old	8-week-old	10-week-old	5-week-old	10-week-old	5-week-old
Duration of treatment	4 weeks	2 weeks	6 weeks	4 weeks	6 weeks	4 weeks
Outcome	VM volume reduction: 32.4% at 2 weeks; 65% at 4 weeks. Normalization of phlebectasias in portal vein and inferior *vena cava*. Cessation of bleeding of lesion after 1 week of treatment. VM no longer detected upon necropsy 4 weeks after treatment.	No volume reduction, mouse became ill after 2 weeks and had to be sacrificed in line with UK Home Office regulations.	VM volume reduction: 18.7% at 2 weeks, 28.4% at 4 weeks, 37% at 6 weeks. Cessation of rectal bleeding immediately after treatment	Normalization of portal vein and inferior *vena cava* phlebectasia	Overall healthy	Overall healthy

* Mice were treated with rapamycin, 4 mg/kg every other day

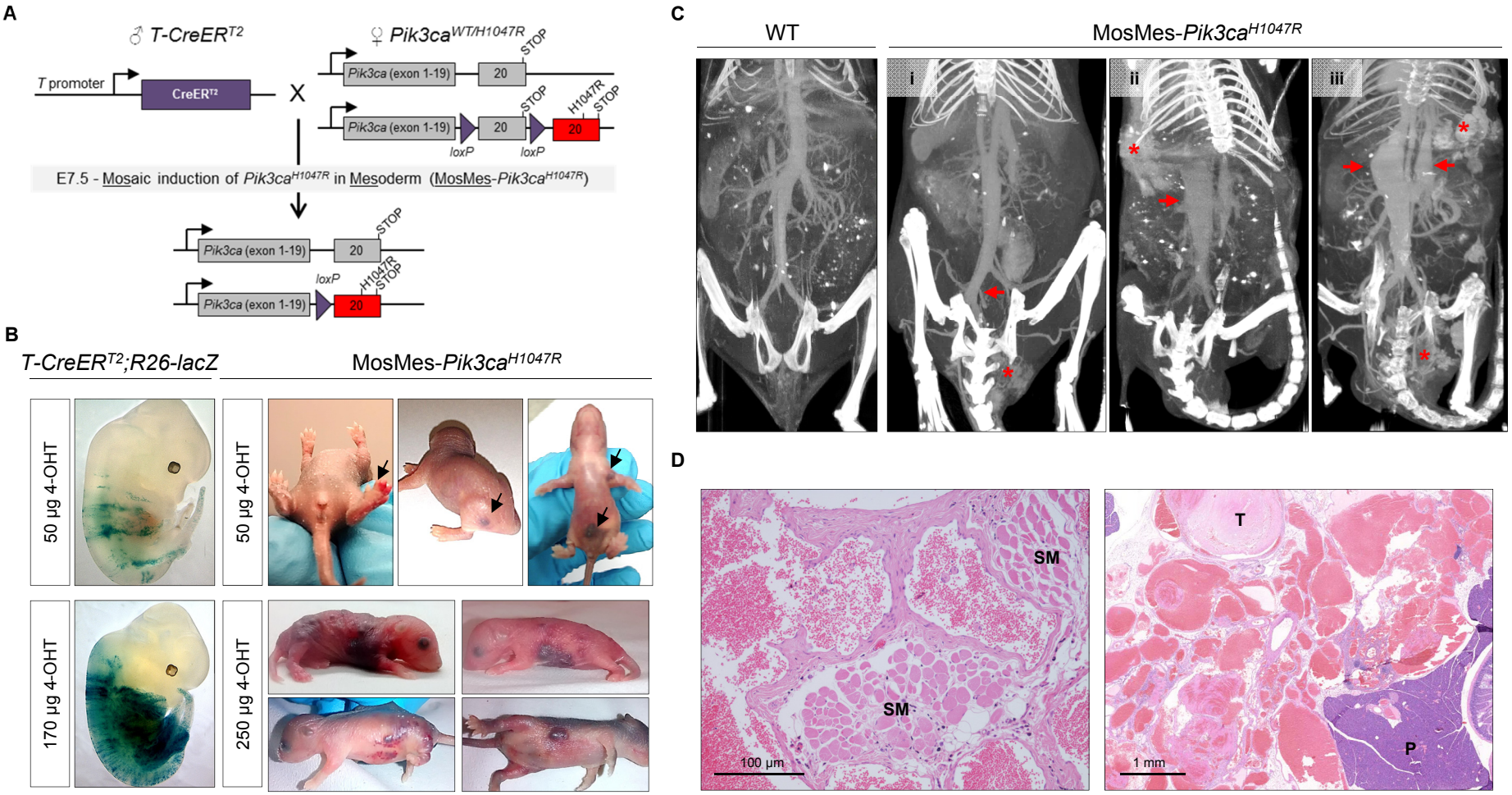
A
♂ T-CreER^{T2}
♀ Pik3ca$^{WT/H1047R}$
T promoter
CreER^{T2}
X
Pik3ca (exon 1-19)
20
STOP
loxP
H1047R
E7.5 - Mosaic induction of Pik3ca^{H1047R} in Mesoderm (MosMes-Pik3ca^{H1047R})
B
T-CreER^{T2};R26-lacZ
MosMes-Pik3ca^{H1047R}
50 µg 4-OHT
170 µg 4-OHT
250 µg 4-OHT
C
WT
MosMes-Pik3ca^{H1047R}
i
ii
iii
D
SM
100 µm
T
P
1 mm


A
B

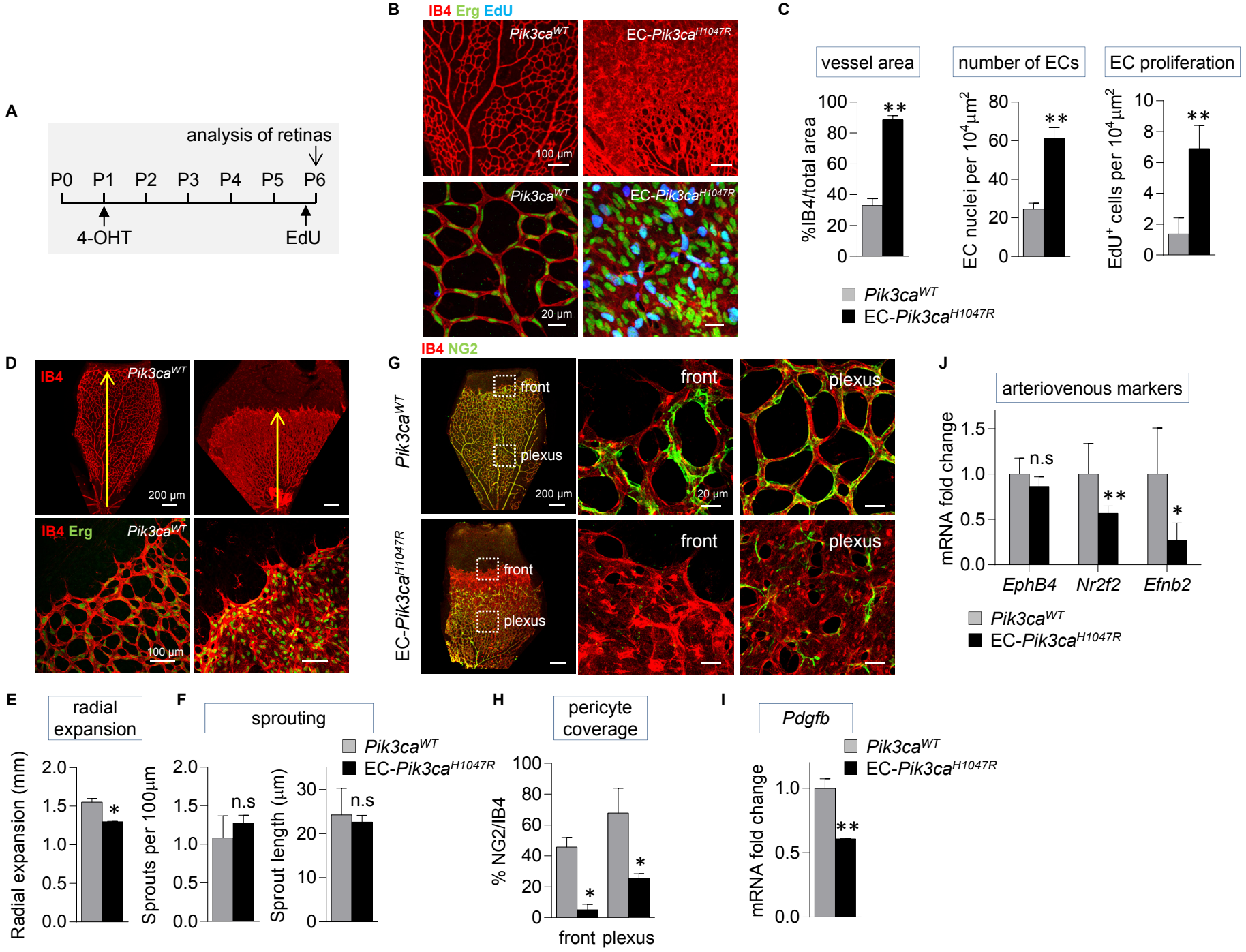
A
analysis of retinas
P0 P1 P2 P3 P4 P5 P6
4-OHT
EdU
B
IB4 Erg EdU
Pik3ca^WT
EC-Pik3ca^H1047R
100 µm
20 µm
C
vessel area
number of ECs
EC proliferation
%IB4/total area
EC nuclei per 10^4µm^2
EdU+ cells per 10^4µm^2
**
Pik3ca^WT
EC-Pik3ca^H1047R
D
IB4
IB4 Erg
200 µm
100 µm
G
IB4 NG2
front
plexus
200 µm
20 µm
J
arteriovenous markers
mRNA fold change
n.s
EphB4
Nr2f2
Efnb2
E
radial expansion
Radial expansion (mm)
F
sprouting
Sprouts per 100µm
Sprout length (µm)
H
pericyte coverage
% NG2/IB4
front plexus
I
Pdgfb
mRNA fold change

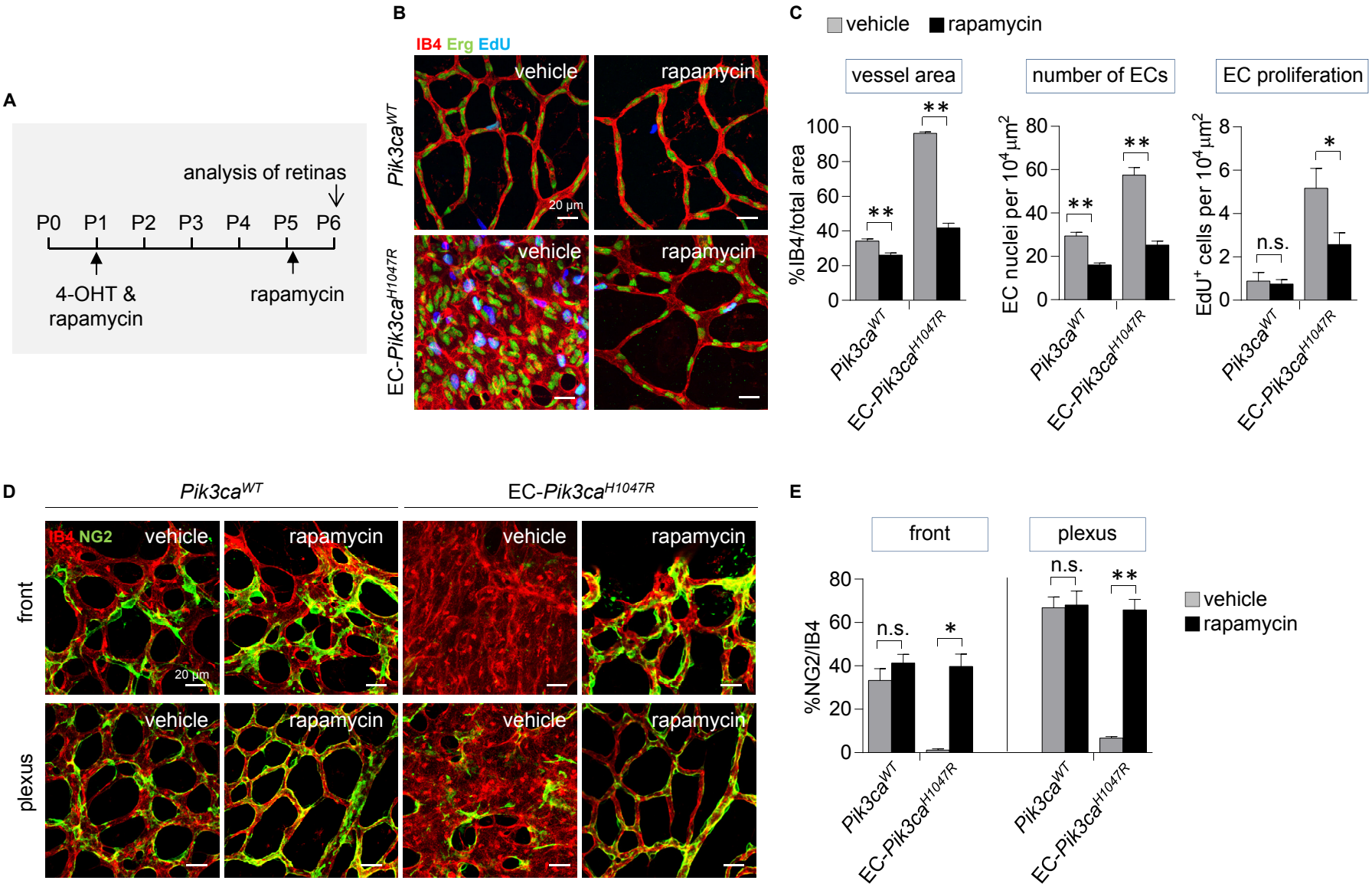
A
analysis of retinas
P0 P1 P2 P3 P4 P5 P6
4-OHT &
rapamycin
rapamycin
B
IB4 Erg EdU
Pik3ca^WT
EC-Pik3ca^H1047R
vehicle
rapamycin
20 μm
C
vehicle
rapamycin
vessel area
number of ECs
EC proliferation
%IB4/total area
EC nuclei per 10^4 μm^2
EdU+ cells per 10^4 μm^2
n.s.
**
*
Pik3ca^WT
EC-Pik3ca^H1047R
D
Pik3ca^WT
EC-Pik3ca^H1047R
front
plexus
IB4 NG2
E
front
plexus
%NG2/IB4
vehicle
rapamycin

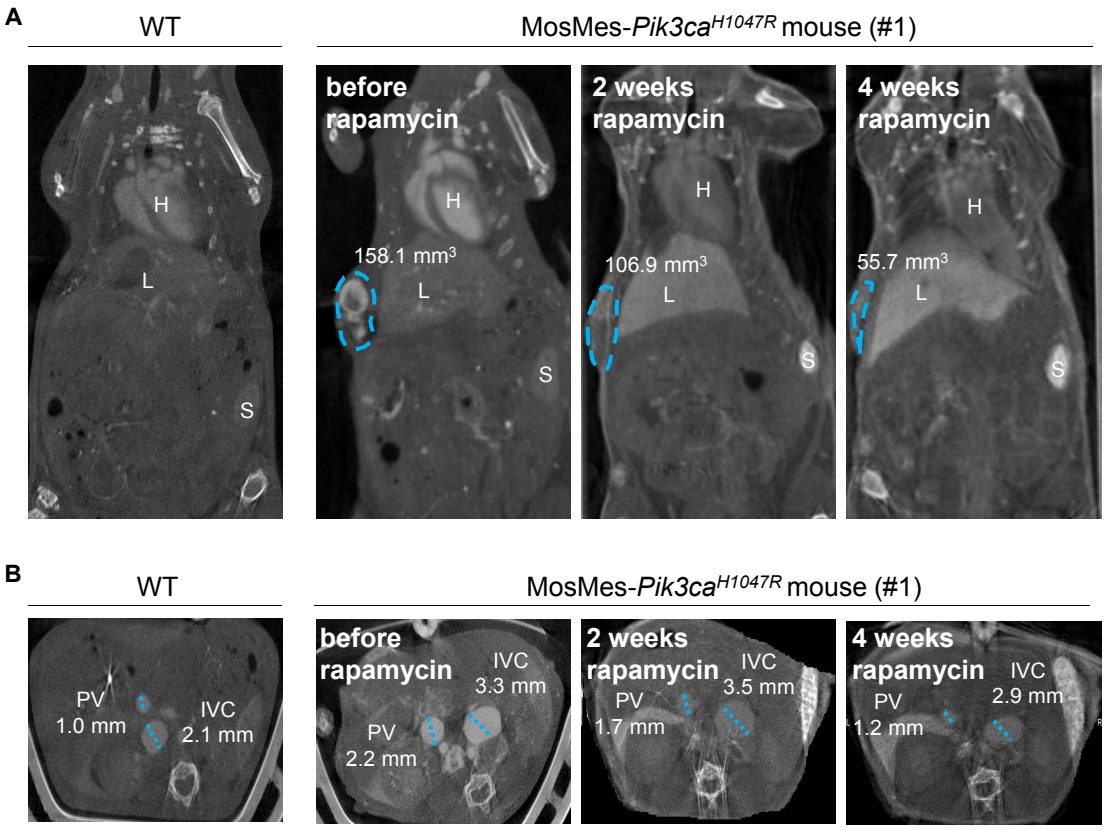
A
WT
MosMes-Pik3ca^H1047R mouse (#1)
H
L
S
before rapamycin
158.1 mm3
2 weeks rapamycin
106.9 mm3
4 weeks rapamycin
55.7 mm3
B
WT
MosMes-Pik3ca^H1047R mouse (#1)
PV 1.0 mm
IVC 2.1 mm
before rapamycin
PV 2.2 mm
IVC 3.3 mm
2 weeks rapamycin
PV 1.7 mm
IVC 3.5 mm
4 weeks rapamycin
PV 1.2 mm
IVC 2.9 mm

A

pTcreER^{T2} vector

B

T-CreER^{T2}; Rosa26-LacZ

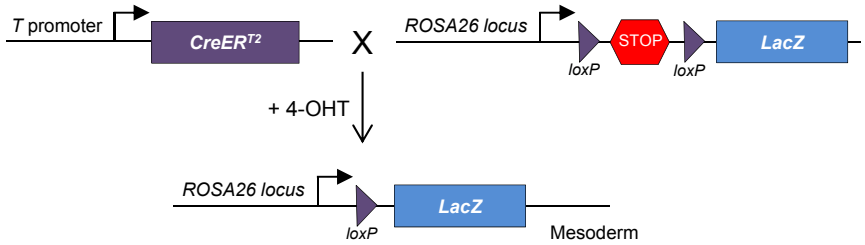

C

Embryonic day (E) of induction of T-CreER^{T2} (500 µg of 4-OHT)

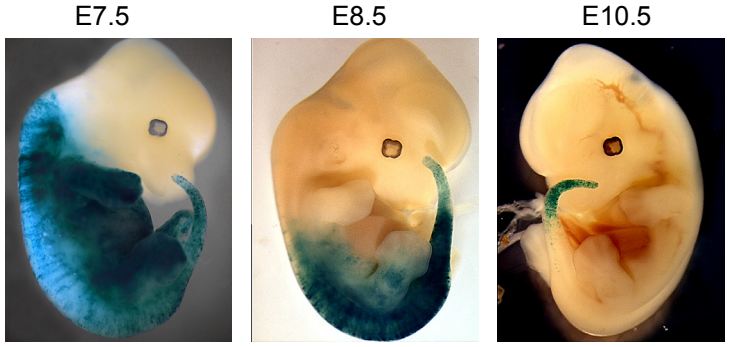

D

Induction of T-CreER^{T2} at E7.5 (µg of 4-OHT)

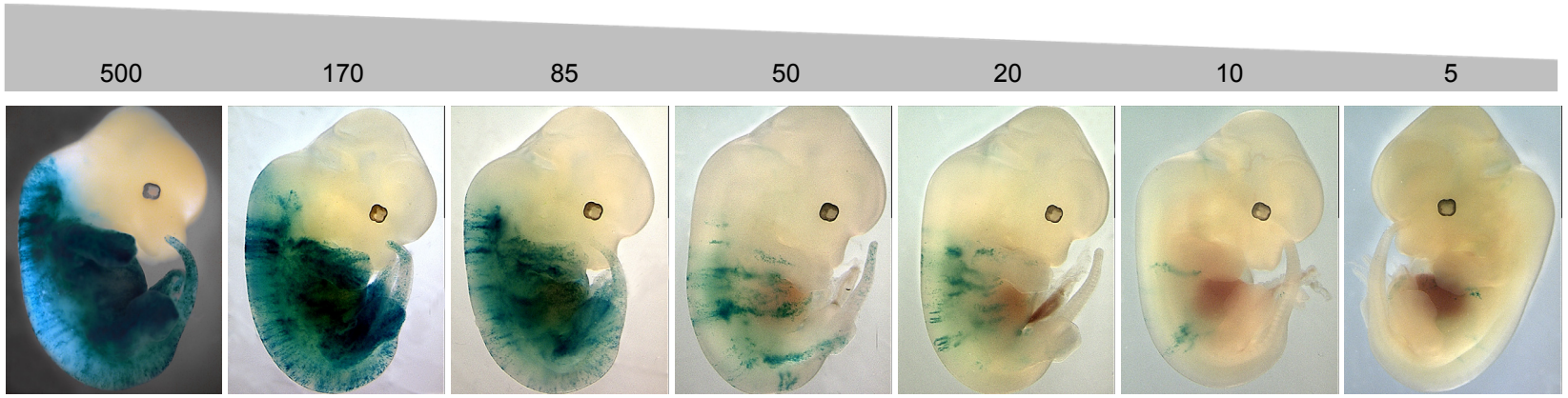

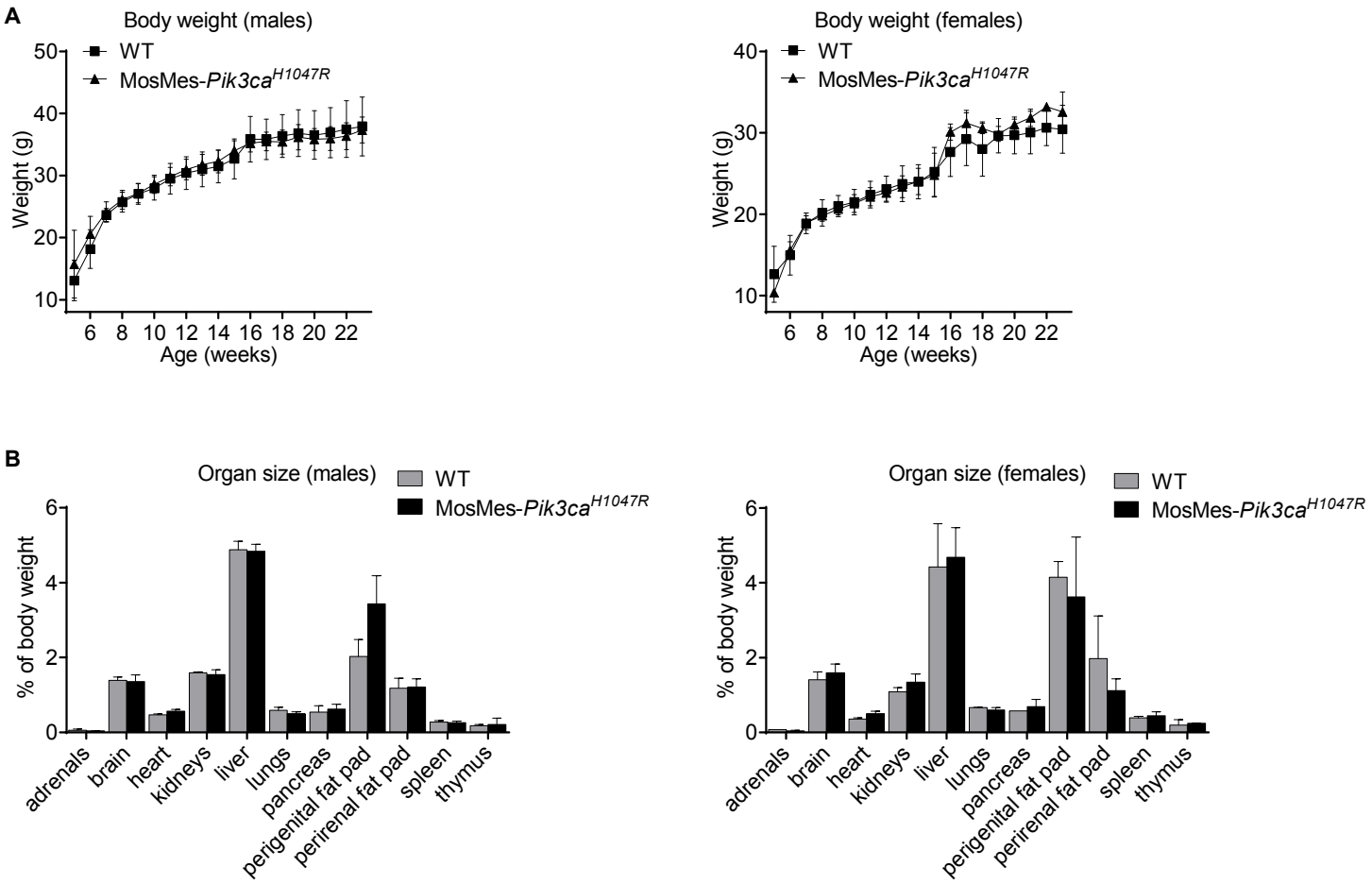
A
Body weight (males)
WT
MosMes-Pik3ca H1047R
Weight (g)
Age (weeks)
Body weight (females)
WT
MosMes-Pik3ca H1047R
Weight (g)
Age (weeks)
B
Organ size (males)
WT
MosMes-Pik3ca H1047R
% of body weight
adrenals
brain
heart
kidneys
liver
lungs
pancreas
perigenital fat pad
perirenal fat pad
spleen
thymus
Organ size (females)
WT
MosMes-Pik3ca H1047R
% of body weight
adrenals
brain
heart
kidneys
liver
lungs
pancreas
perigenital fat pad
perirenal fat pad
spleen
thymus

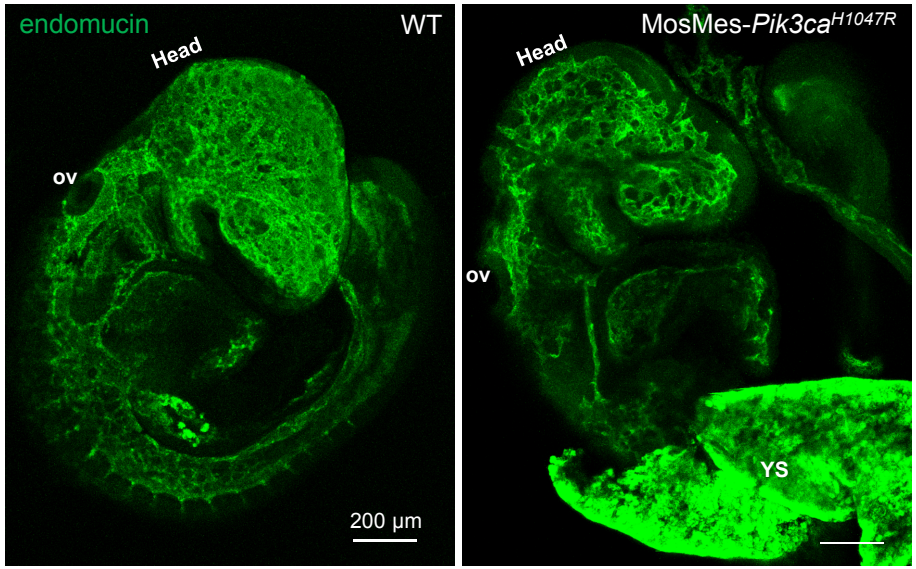
endomucin
WT
Head
ov
200 µm
Head
MosMes-*Pik3ca*^{H1047R}
ov
YS

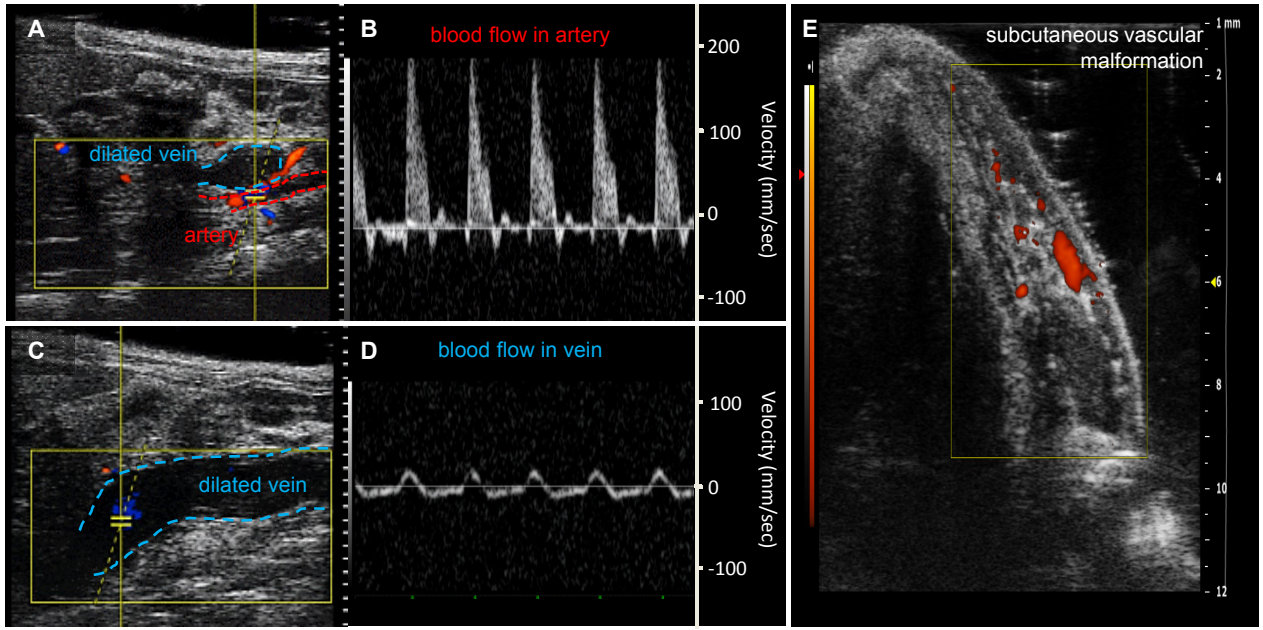
A
dilated vein
artery
B
blood flow in artery
200
100
0
-100
Velocity (mm/sec)
C
dilated vein
D
blood flow in vein
100
0
-100
Velocity (mm/sec)
E
subcutaneous vascular malformation
1 mm
2
4
6
8
10
12

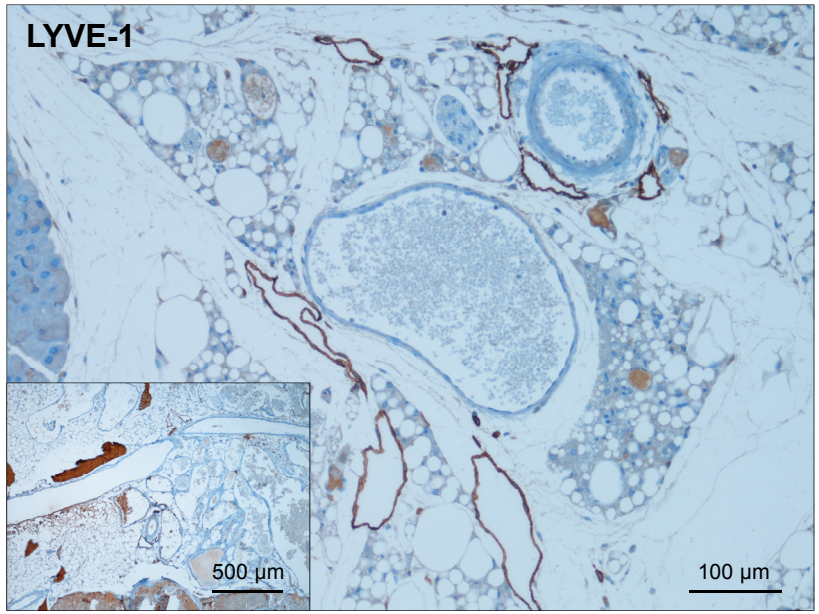
LYVE-1
500 µm
100 µm

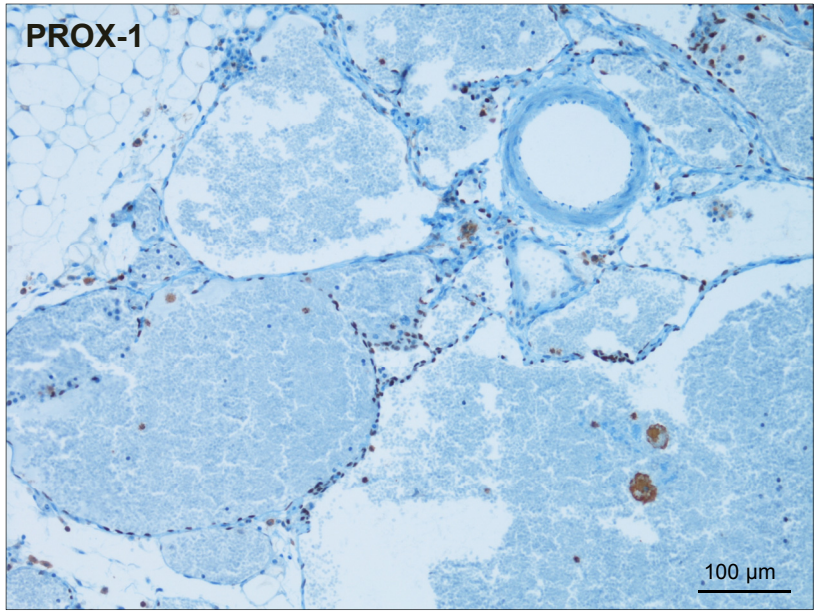
PROX-1
100 µm

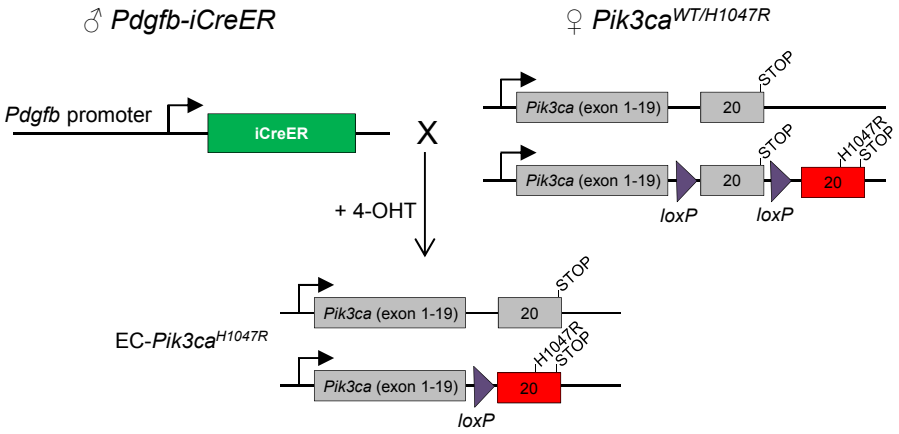
♂ Pdgfb-iCreER
♀ Pik3ca WT/H1047R
Pdgfb promoter
iCreER
X
+ 4-OHT
Pik3ca (exon 1-19)
20
STOP
H1047R
loxP
EC-Pik3ca H1047R

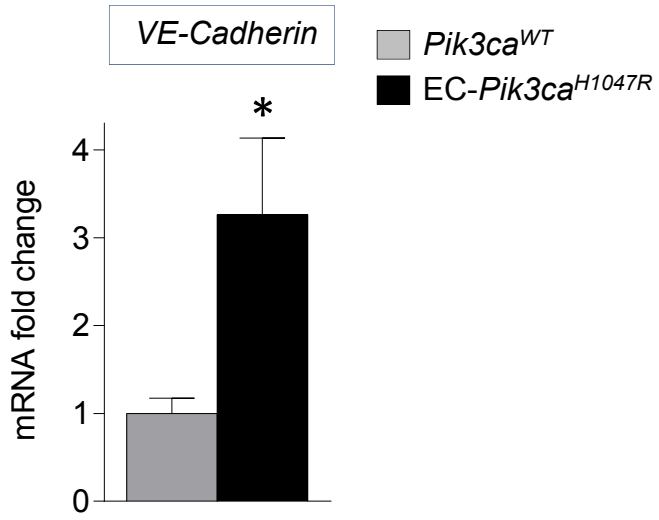
VE-Cadherin
Pik3ca^WT
EC-Pik3ca^H1047R
mRNA fold change
0
1
2
3
4
*

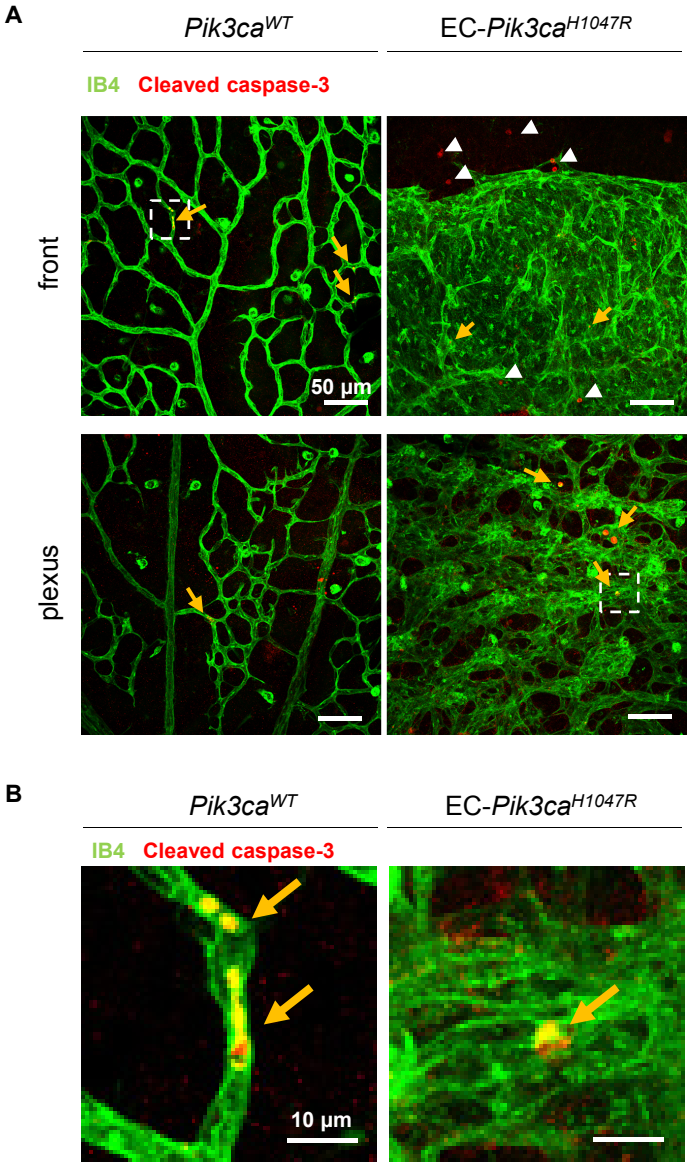
A
Pik3ca^WT
EC-Pik3ca^H1047R
IB4 Cleaved caspase-3
front
plexus
50 μm
B
Pik3ca^WT
EC-Pik3ca^H1047R
IB4 Cleaved caspase-3
10 μm

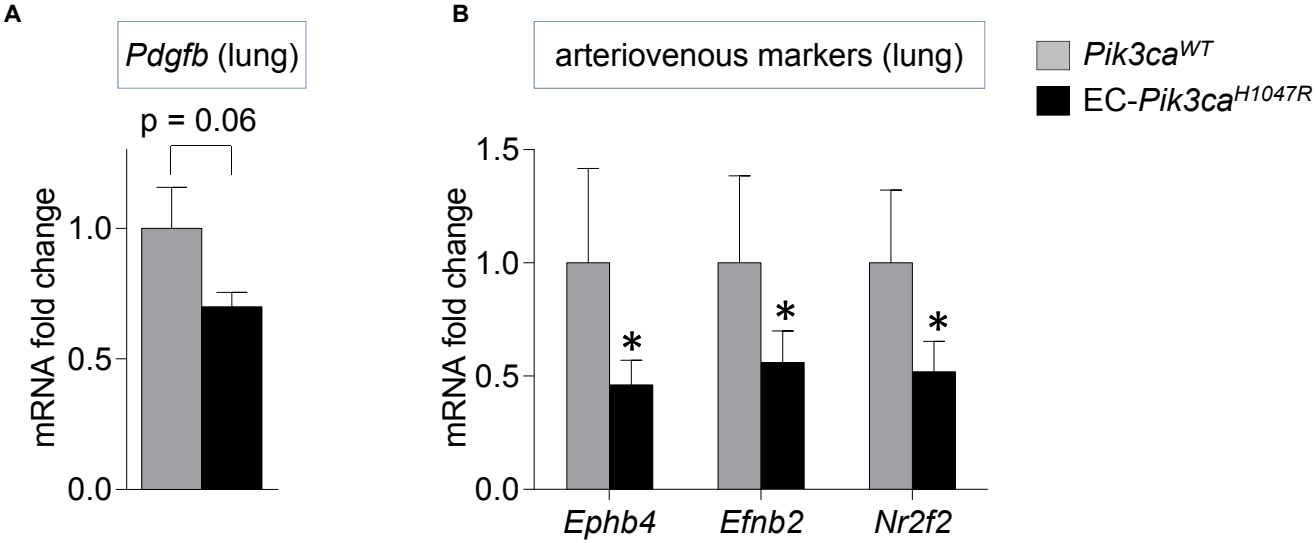
A
Pdgfb (lung)
p = 0.06
mRNA fold change
1.0
0.5
0.0
B
arteriovenous markers (lung)
Pik3ca^WT
EC-Pik3ca^H1047R
mRNA fold change
1.5
1.0
0.5
0.0
*
*
*
Ephb4
Efnb2
Nr2f2

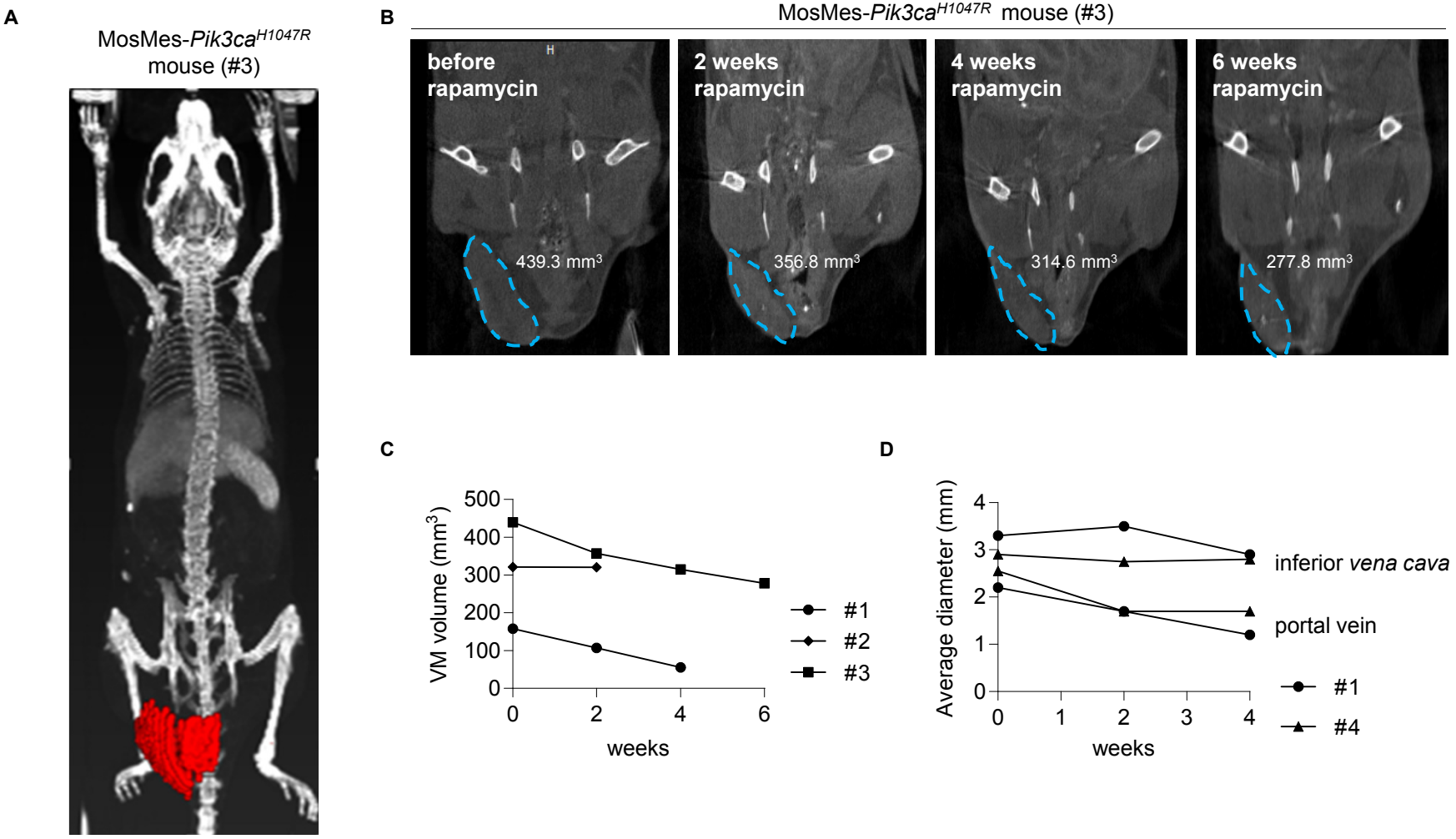
A
MosMes-Pik3ca^H1047R mouse (#3)
B
MosMes-Pik3ca^H1047R mouse (#3)
before rapamycin
439.3 mm3
2 weeks rapamycin
356.8 mm3
4 weeks rapamycin
314.6 mm3
6 weeks rapamycin
277.8 mm3
C
VM volume (mm3)
500
400
300
200
100
0
0
2
4
6
weeks
#1
#2
#3
D
Average diameter (mm)
4
3
2
1
0
0
1
2
3
4
weeks
inferior vena cava
portal vein
#1
#4

Supplementary Material

Figure S1

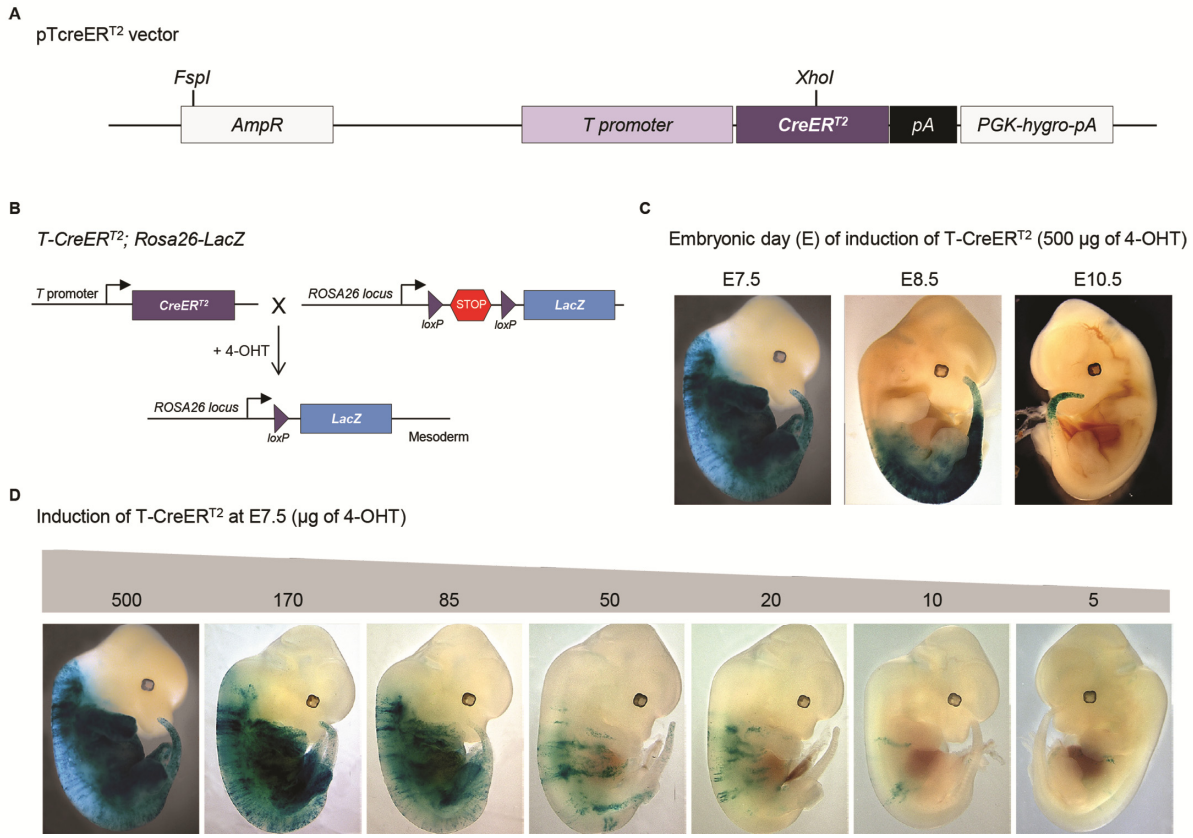

Figure S1. Cre-mediated mosaic recombination in the *T-CreER^{T2}* mouse line. (**A**) Schematic representation of the pTcreER^{T2} transgene used for the generation of the *T-CreER^{T2}* mouse line. (**B**) Cre-mediated recombination of the *Rosa26-lacZ* reporter inducing β-gal activity. (**C**) Whole-mount images of E12.5 *T-CreER^{T2};Rosa26-lacZ* embryos, stained for β-gal after 4-OHT administration at E7.5, E8.5, or E10.5. (**D**) Same as in (C) but after administration of different doses of 4-OHT (5 to 500 µg) at E7.5.

Figure S2

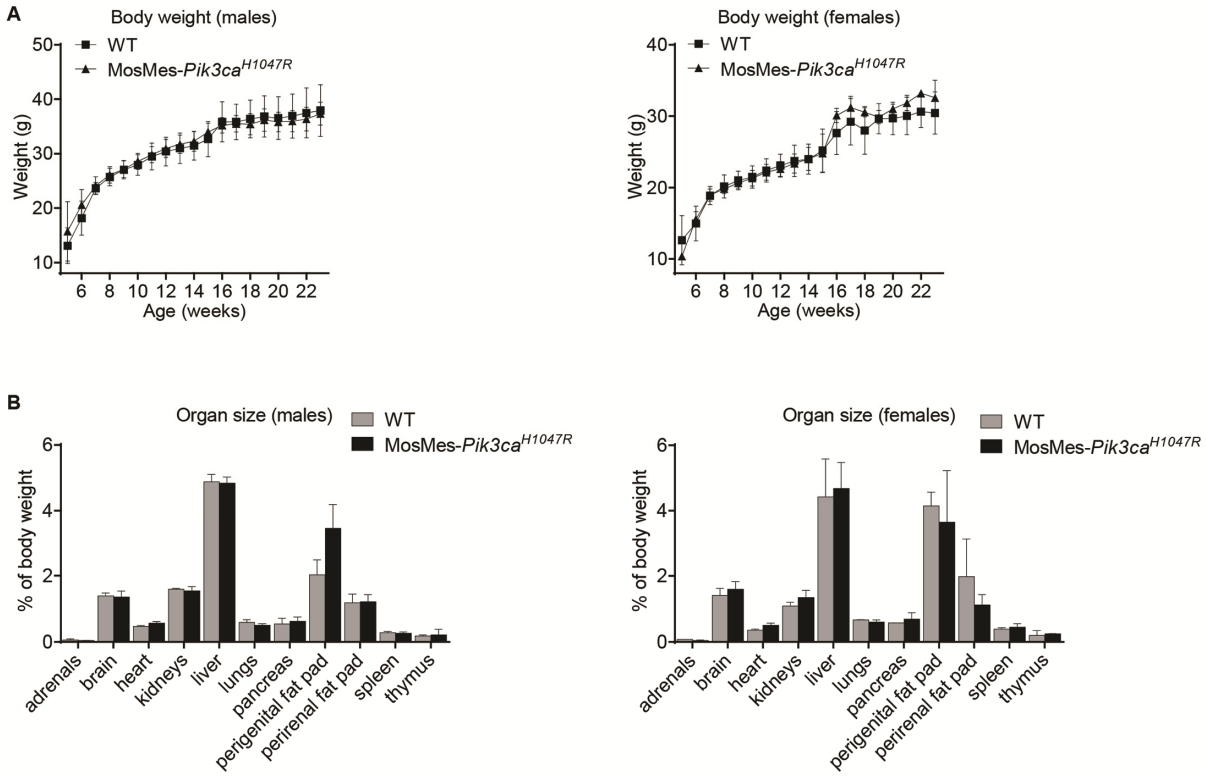

Figure S2. Body weight and organ size of WT and MosMes-*Pik3ca*^{H1047R} mice. Body weight over time (**A**) and organ size at 6 months of age (**B**) were measured for WT and MosMes-*Pik3ca*^{H1047R} mice. Data represent mean ± SEM, n=30/genotype for (A), n=6/genotype for (B).

Figure S3

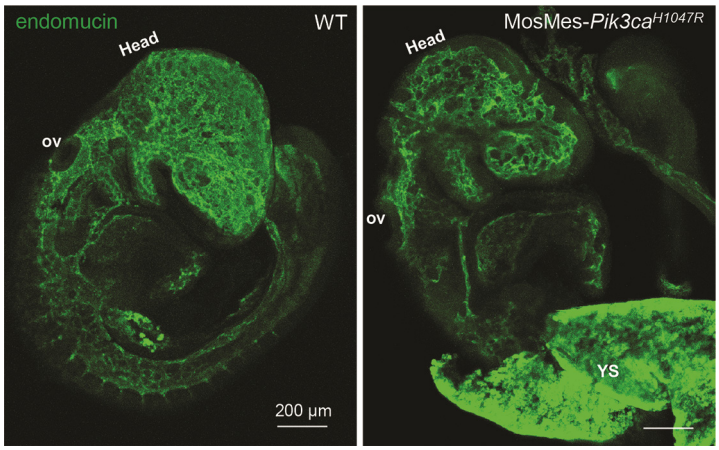

Figure S3. Whole-mount endomucin-staining of E9.5 embryos dosed with 170 µg 4-OHT at E7.5. The MosMes-*Pik3ca*^{H1047R} embryo shows an overall less developed vasculature compared to the WT embryo. ov, otic vesicle; YS, yolk sac.

Figure S4

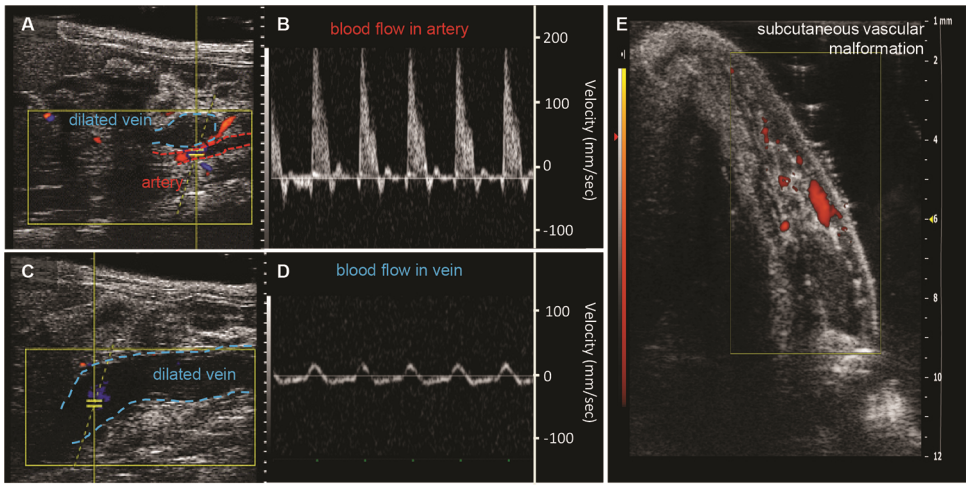

Figure S4. MosMes-*Pik3ca*^{H1047R} mouse with a subcutaneous vascular malformation and dilated vein. (**A,C**) Ultrasound images with color Doppler showing artery (red dashed line) and dilated vein (blue dashed line) of a MosMes-*Pik3ca*^{H1047R} mouse. Yellow markers indicate the region from which pulsed wave Doppler was acquired. (**B,D**) Pulsed wave Doppler measurement of blood flow demonstrates a high arterial flow velocity wave form within the artery (B) and a slow venous flow velocity wave form within the dilated vein (D). (**E**) Power Doppler ultrasound demonstrates slow flow signals in subcutaneous vascular malformation.

Figure S5

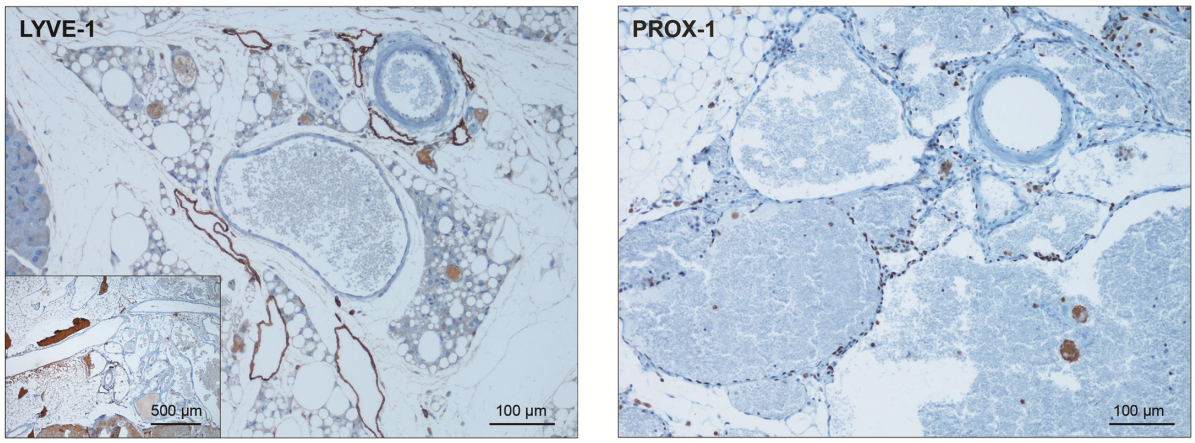

Figure S5. **Immunostaining for lymphatic markers in VMs of MosMes-*Pik3ca*^{H1047R} mice.** Left, representative image of LYVE-1 immunostaining. Right, representative image of PROX-1 immunostaining.

Figure S6

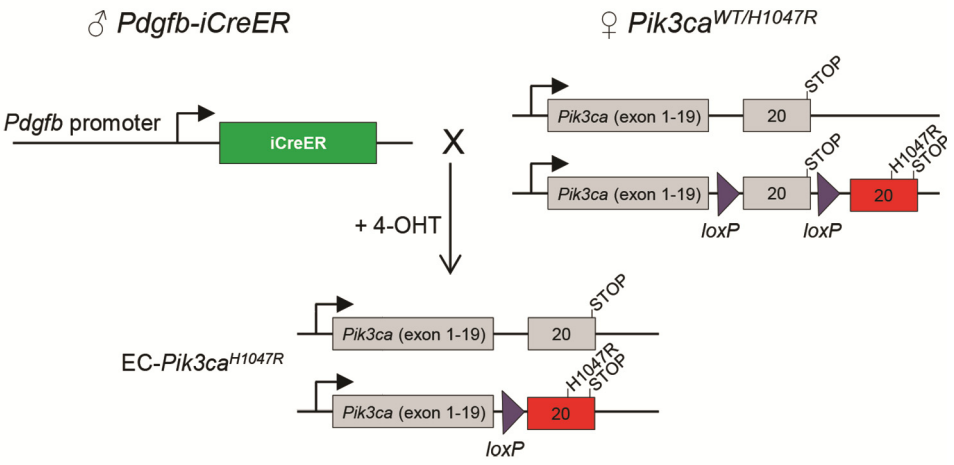

Figure S6. Genetic strategy for activating *Pik3ca*^{H1047R} in ECs. *Pdgfb-iCreER* mice were crossed with *Pik3ca*$^{WT/H1047R}$ mice.

Figure S7

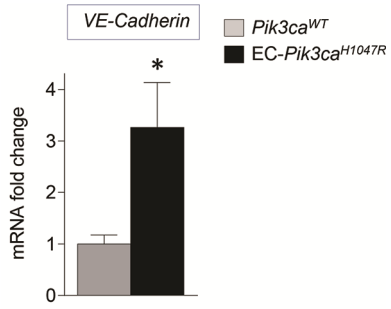

Figure S7. **Expression of *VE-Cadherin* in P6 EC-*Pik3ca*^{H1047R} retinas.** *VE-Cadherin* mRNA expression was normalized to *Hprt*. Data represent mean ± SEM. *p < 0.05 (Mann-Whitney U test). n=5/genotype.

Figure S8

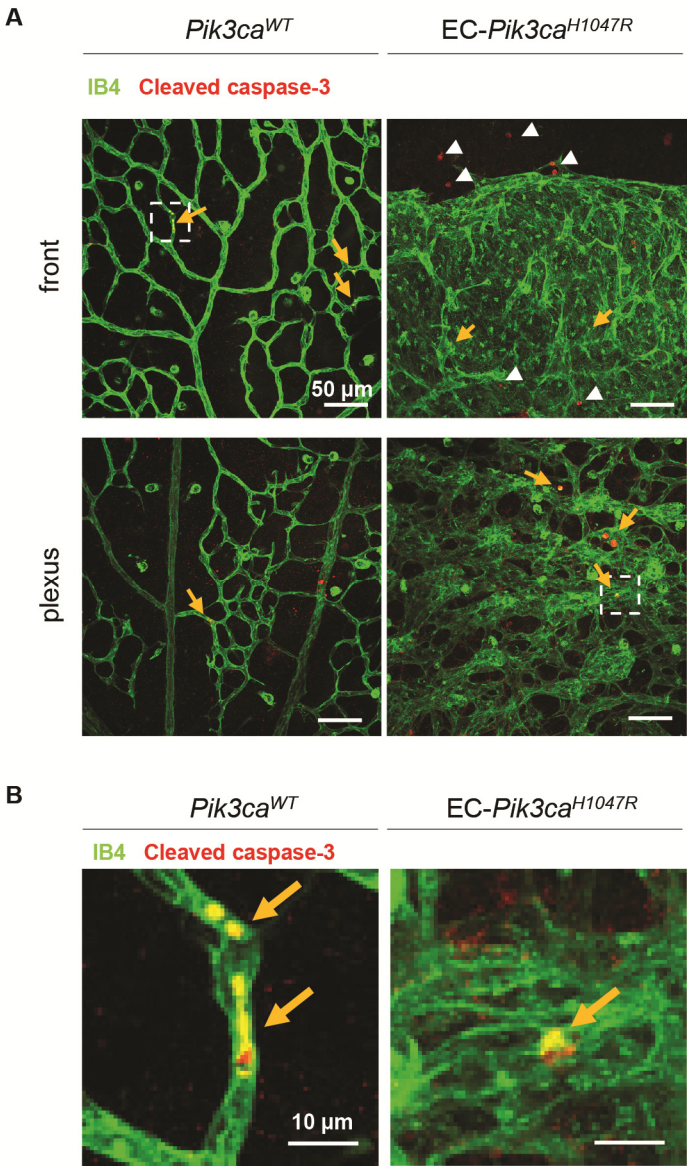

Figure S8. Apoptosis in P9 EC-*Pik3ca*^{H1047R} retinas. (A) Representative flat-mounted *Pik3ca*^{WT} and EC-*Pik3ca*^{H1047R} P9 retinas, stained with IB4 (green, revealing ECs) and with antibody to cleaved caspase-3 (marker of apoptosis; red). Indicated are apoptotic ECs (orange arrows) and non-EC apoptotic cells (white arrowheads). (**B**) Higher magnification of sections highlighted in (A).

Figure S9

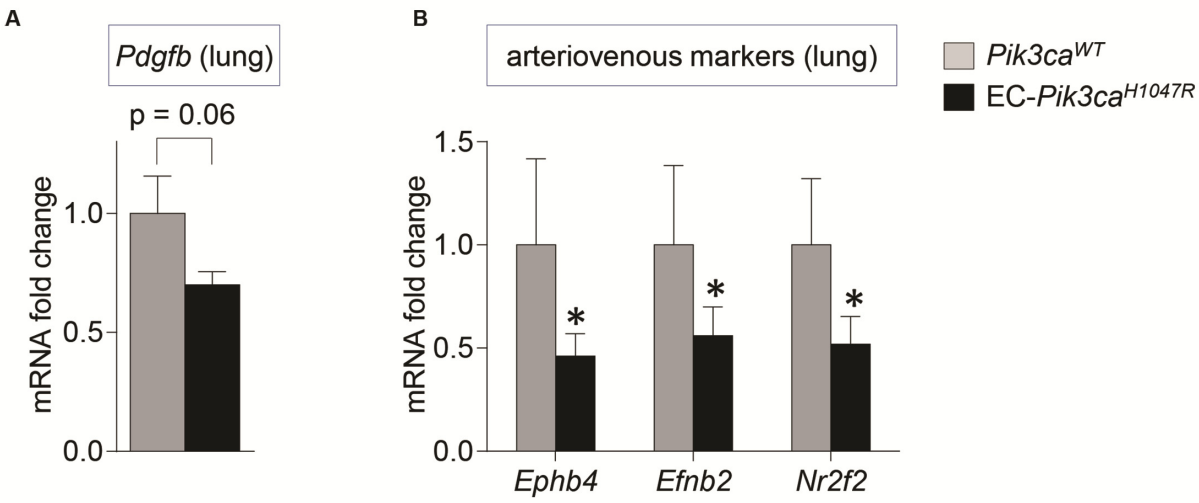

Figure S9. Expression of *Pdgfb* and arteriovenous markers in EC-*Pik3ca*^{H1047R} lungs. (**A**) Expression of *Pdgfb* in EC-*Pik3ca*^{H1047R} lungs. Data represent mean ± SEM (Mann-Whitney U test). (**B**) Expression of *Ephb4*, *Efnb2,* and *Nr2f2* mRNA in lung lysates of *Pik3ca*^{WT} and EC-*Pik3ca*^{H1047R} P6 mice. Data represent mean ± SEM. *p < 0.05 (Mann-Whitney U test). n=5/genotype.

Figure S10

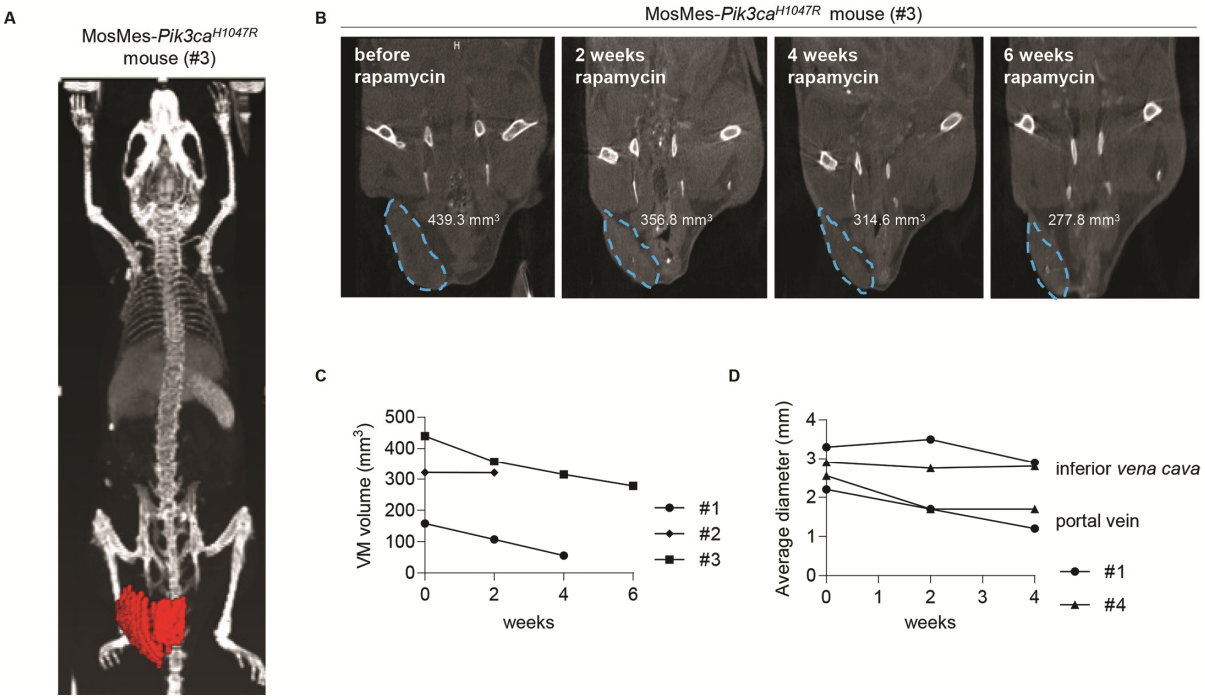

Figure S10. Treatment of MosMes-*Pik3ca*^{H1047R} mice with rapamycin. (**A**) 3D image reconstruction of CT-A of MosMes-*Pik3ca*^{H1047R} mouse #3 before treatment, subcutaneous VM highlighted in red. (**B**) CT-A images of MosMes-*Pik3ca*^{H1047R} mouse #3 upon rapamycin treatment showing the volume of the subcutaneous VM (circled in blue). (**C**) Graph showing volumes of VM from MosMes-*Pik3ca*^{H1047R} mice during rapamycin treatment. (D) Graph showing average diameter of inferior vena cava and portal vein of MosMes-*Pik3ca*^{H1047R} mice during rapamycin treatment.

Supplementary Table 1. List of organs and tissues subjected to histological examination.

The organs were examined by H&E staining in WT and MosMes-*Pik3ca*^{H1047R} mice.

Adrenals	Ovaries/oviducts
Aorta	Pancreas
Brain	Parathyroid
Cecum	Prostate
Cervix	Rectum
Colon	Salivary gland
Duodenum	Seminal vesicles
Epididymis	Skeletal muscle
Esophagus	Skin
Eyes	Spleen
Perigenital fat pad	Sternum
Perirenal fat pad	Stomach
Femur	Submandibular lymph nodes
Heart	Testes
Ileum	Thymus
Jejunum	Thyroids
Kidneys	Tongue
Liver	Trachea
Lungs	Urinary bladder
Mammary glands	Uterus/vagina

Supplementary Table 2. Percentage of MosMes-*Pik3ca*^{H1047R} mice with VMs after dosing with different doses of 4-OHT.

µg 4-OHT administered per pregnant mouse	MosMes-*Pik3ca*^{H1047R} mice with VMs
12.5	12.5%
50	15%
250	100%

Supplementary Table 3. Percentage of live WT and MosMes-*Pik3ca*^{H1047R} offspring after different doses of 4-OHT. The expected normal Mendelian distribution is 50% of each genotype.

	observed frequency	
µg 4-OHT administered per pregnant mouse	WT	MosMes-*Pik3ca*^{H1047R}
12.5	50.0%	50.0%
50	48.7%	51.3%
250	61.5%	38.5%